EFFECT OF OFF-FAULT LOW-VELOCITY ELASTIC INCLUSIONS ON SUPERSHEAR RUPTURE DYNAMICS

BY

XIAO MA

THESIS

Submitted in partial fulfillment of the requirements
for the degree of Master of Science in Civil Engineering
in the Graduate College of the
University of Illinois at Urbana-Champaign, 2014

Urbana, Illinois

Adviser:

Professor Ahmed E. Elbanna

Abstract

The velocity structure in the lithosphere is generally heterogeneous. Wave reflection, transmission, and diffraction from the boundaries of the different layers and inclusions are expected to affect rupture propagation on faults embedded in these heterogeneous structures. Here,a model of dynamic rupture on a frictional fault embedded in an elastic full space is presented, governed by plane strain elasticity, with an off-fault inclusion that has a lower rigidity than the background medium. The elastodynamics problem is solved by using the Finite Element software Pylith. The fault operates under linear slip-weakening friction law. Initiate the rupture by artificially overstressing a localized region near the left edge of the fault, considering embedded soft inclusions with 20% to 60% reduction in both of the shear and pressure wave speeds. The embedded inclusions are placed at different distances from the fault surface and have different dimensions. One observation is that the existence of a soft inclusion may significantly shorten the transition length to supershear propagation through the Burridge-Andrews mechanism. The higher the material contrast, the shorter the transition length to supershear propagation becomes. Another observation is that supershear rupture is generated at pretress values that are lower than what is theoretically predicted for a homogeneous medium. The implications of the results for dynamic rupture propagation in complex velocity structures as well as supershear propagation on understressed faults are discussed.

To my parents, Wenli and Xiao Ke

Acknowledgments

First and foremost, I would like to express my deep gratitude to my advisor Professor Ahmed. E. Elbanna, without Ahmed this work could not be finished. Ahmed is a great mentor and a friend. He is always there for me, even for my naive questions. I am impressed that Ahmed is so knowledgeable and enthusiastic about scientific research. He is always encouraging me to develop my potential. It is always a pleasure to work with Ahmed.

I acknowledge the support from the National Science Foundation NSF EAR 13-45108.

I am thankful for my colleagues, specifically I want to thank Darin Peetz for his support in terms of academics and friendship.

Additionally, I am grateful for all my friends, specifically Xiaojia Zhang, Haoyang Li, thank you for making my life colorful and filled with happiness.

Finally, I would like to thank my father Wenli Ma and my mother Xiao Ke for all these years caring and loving. I am so lucky to have the best parents in the world, they are my rock, helping me go though all the difficulties. To my parents, I dedicate this work.

TABLE OF CONTENTS

LIST OF TABLES

LIST OF FIGURES

CHAPTER 1

Introduction

The velocity structure in the vicinity of pre-existing fault networks is, in general, heterogeneous [2]. In particular, faults zones are usually composed of rocks and granular materials that have experienced different cycles of damage and healing. This leads to time dependent variations in the magnitude of elastic moduli and the wave speeds [3]. The existence of a heterogeneous material structure is expected to affect rupture propagation on the embedded fault segments due to wave reflection, transmission and diffraction from the boundaries of the different layers and inclusions.

Of the different complexities that may arise in the velocity structure near pre-existing faults, the properties of low-velocity zones (LVZs) have been extensively studied. Examples include LVZs around San Andreas [4, 5, 6], San Jacinto [7, 8], Landers [9, 10, 11], Hector Mine [12], Calico [13, 14], Nojima [15], and North Anatolian [16] fault zones.

The implications of the existence of a LVZ adjacent to the fault surface, within an otherwise homogeneous medium, have been explored using spontaneous dynamic rupture models [17, 18, 19, 20, 21]. The velocity reduction within the LVZ, relative to the country rock, may vary in the range of 20%-60%. It was found that the trapped waves in the low velocity zone alter the shear stress on the fault plane and affect both the dynamic rupture mode [20] and rupture characteristics including supershear propagation [18, 20, 21]. The enhanced supershear transition observed in simulations with LVZs [21] suggests that more heterogeneous velocity structure must be considered when investigating rupture speed.

Supershear rupture propagation has been inferred from seismic observations for natural faults. in several large strike-slip earthquake, including the

1979 Imperial Valley earthquake [22, 23], the 1999 Kocaeli (Izmit) earthquake [24, 25], the 1999 Duzce earthquake [22, 25, 26], the 2001 Kokoxili (Kunlun) earthquake [27, 28, 29, 30], and the 2002 Denali earthquake [31, 32].

The transition from rupture velocity less than Rayleigh velocity to rupture velocity greater than shear wave velocity has been studied using dynamic rupture simulations [33, 34, 35, 36, 37, 38, 19, 39, 40, 41, 42, 43, 44, 45, 46, 47, 48, 49, 50, 51, 21, 52]. The primary mechanism for the supershear transition is known as Burridge-Andrews mechanism [33, 34] in which a daughter crack is nucleated at the S wave shear stress peak ahead of the propagating Mode II rupture.

In order for the Burridge-Andrews mechanism to take place on a homogeneous fault in 2-D models, the prestress must be high enough. The strength parameter S [34, 35] has to be smaller than $S_{crit} = 1.77$. Previous work has shown that heterogeneities on the fault surface, including variations in the prestress or fracture energy, may enable supershear propagation at lower prestress values than what are theoretically predicted under homogeneous conditions. The effect of off-fault heterogeneities in the form of off-fault plasticity and damage has also been recently investigated [21]. The influence of off-fault material heterogeneities, as may be represented by inclusions or layered structure, is the focus of this paper.

Material gradient and contrasts may not be confined to the vicinity of fault surfaces. Velocity anomalies in the form of lenses with lower or higher wave speeds than the surrounding medium may exist at some distance from the fault surface. In this case, additional interfaces, introduced by the boundaries of the domain with the different rigidity, produce multiple reflections in the wave field as well as diffraction and refraction effects. These modulations may influence the rupture process and increase the complexity of the dynamic response.

In this paper a model dynamic rupture propagation on a slip weakening fault in an elastic domain with an embedded inclusion of a lower rigidity is investigated. This softer inclusion may not be directly adjacent to the fault surface and it may have a limited extension relative to the fault length.

Chapter 2 describes the model setup and parameters selection. In Chapter 3 the simulation results are presented regarding the influence of the embedded soft inclusion on the supershear transition as well as rupture propagation characteristics. Examination is carried out about the robustness of the findings with respect to variations in the soft inclusion thickness, the off-fault distance, material contrast degree and the stress level effect. In Chapter 4, discussion is made about the implications of the results in the context of other observational and computational models involving LVZs and supershear ruptures.Summarization of the conclusions is made in Chapter 5.

CHAPTER 2

Model Setup

A planar fault in a linear elastic isotropic medium under inplane strain conditions is considered. The medium has a shear modulus μ_1 everywhere except for the inclusion that possesses a smaller shear modulus μ_2 . The inclusion geometry is chosen to be rectangular with a width H_2, a length H_3 , and is located at a distance H_1 from the fault. The medium geometry is symmetric about the fault plane. Absorbing boundary conditions are applied at the four boundaries of the domain to mimic an infinite extension in all direction.

The fault friction is governed by linear slip-weakening law [53, 54] where the frictional shear strength Γ decreases linearly as a function of slip δ from its static value τ_s to the dynamic value τ_d over a characteristic slip d_c (Eqn. 2.1).The friction law parameters are kept the same in all the simulations. Choose the static friction coefficient to be 0.6, the dynamic friction coefficients to be 0.5 and the characterize slip weakening distance to be 0.2m

$$\Gamma(\delta) = \begin{cases} \tau_d + (\tau_s - \tau_d)/(1 - \delta/d_c), \delta \leq d_c \\ \tau_d, \delta < d_c \end{cases} \tag{2.1}$$

The static strength τ_s and the dynamic strength τ_d are the products of the effective normal stress by the corresponding static and dynamic friction coefficients, respectively. The implications of the choice of this particular friction law compared to other formulations, such as rate and state friction, are discussed in chapter 4.

Solve the dynamic rupture problem under 2-D plane strain conditions using the finite element program Pylith [55]. A uniform mesh with 25 m grid size has been found to be adequate for resolving the process zone within

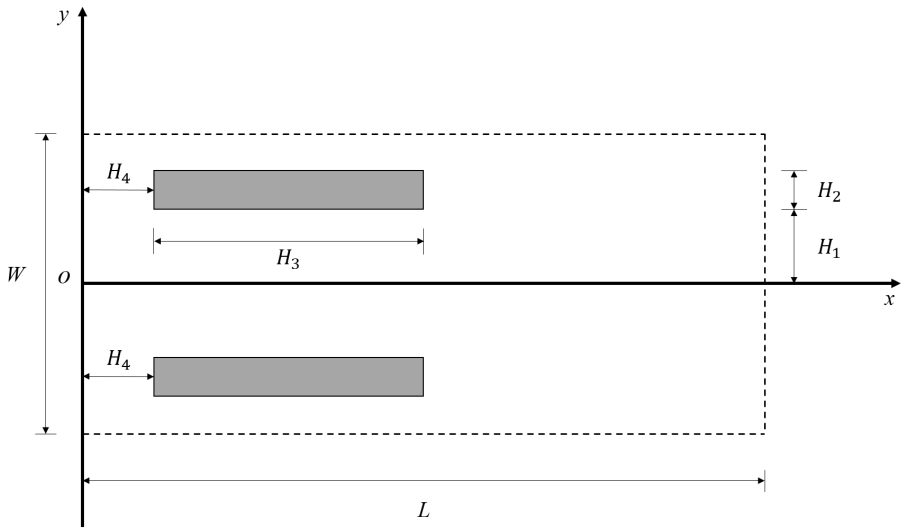

Figure 2.1: The model geometry. The simulated domain has an aspect ratio of L/W. A slip weakening fault of length L bisects the domain and acts as a horizontal symmetry line. Light gray layers represent the location of the soft inclusions. H_1 defines the distance between the fault and the material boundary. H_2 defines the thickness of the soft layer. H_3 defines the length of the soft layer.H_4 defines the off-edge distance of the soft layer inclusion.In most cases investigated here set $H_4 = 0$. Absorbing boundary conditions are used for all edges to simulate an infinite extension in all direction.

the range of parameter values explored in this study. A mesh convergence study is conducted with 12.5 m and 6.25 m element sizes. The results are not affected by the mesh refinement. Table 2.1 summarizes the different parameter values. The fundamental length scale in this problem is given by Eqn. 2.2.

$$L_{nuc} = \frac{\mu_1 d_c}{(\tau_s - \tau_d)} \tag{2.2}$$

where μ_1 is the shear modulus of the homogeneous domain, d_c is the slip weakening distance, τ_s and τ_d are the static and dynamic shear strength values, respectively. This length scale L_{nuc} is proportional to the universal nucleation length predicted for linear slip-weakening friction [56] in a homogeneous medium with a shear modulus μ_1 .

To start the dynamic rupture, overstress the fault beyond its static frictional strength in a limited region extending for 1.5 km to ensure the immediate dynamic propagation. In previous studies, it was pointed out that the nucleation procedure may affect the subsequent dynamic rupture evolution

[39, 42]. The implications of the abrupt nucleation adopted here as compared to other nucleation procedures including quasi-static nucleation are discussed in chapter 4.

Table 2.1: Model Discretization and Constitutive Parameters

Medium and Discretization Parameters	**Value**
Shear Modulus of the background domain, μ	30 GPa
S wave velocity(background),c_s	3.464 $km \cdot s^{-1}$
P wave velocity(background),c_p	6.0 $km \cdot s^{-1}$
Mass density for all layers,ρ	2670 $kg \cdot m^{-3}$
Fault length,L	100 km
Domain width,W	30 km
Fault	$\{x, y \vert y = 0, 0 < x < 100km\}$
Overstress region on the fault	$\{x, y \vert y = 0, 0 < x < 1.5km\}$
Spatial grid space $\Delta x = \Delta y$	25 m
Wave velocity contrast	20-60%
Fault Constitutive Parameters	**Value**
Magnitude of the effective normal stress,σ_n^{eff}	50.0 MPa
Overstressed region initial shear stress	31.0 MPa
Static friction coefficient,μ_s	0.6
Dynamic friction coefficient,μ_d	0.5
Static Strength,τ_s	30.0 MPa
Dynamic Strength,τ_d	25.0 MPa
Strength Parameter,S	Varies
Characteristic slip-weakening distance,d_c	0.2 m

CHAPTER 3

Results

This chapter first examine some observations related to supershear propagation in a homogeneous medium. Then, investigate the influence of the existence of an off-fault low velocity lens on the rupture mode and transition to supershear.

3.1 Supershear rupture propagation in a homogeneous medium

Dunham [40] identified conditions under which supershear transition may occur on a slip weakening fault through the Burridge-Andrews mechanism. Using the strength parameter $S = (\tau_s - \tau_o)/(\tau_o - \tau_d)$ which defines the degree of stressing of the fault relative to its strength limits, Dunham [40] showed that for 2D elasticity, S has to be less than 1.77 in order for the supershear transition to occur under homogeneous conditions. The transition length to supershear increases as the strength parameter value increases and becomes infinite when $S = 1.77$. Verification are made about these findings in the numerical simulations. However, due to the abrupt nucleation procedure adopted here, the transition length is generally smaller than the values predicted by Dunham [40].

Moreover, due to the lack of a healing mechanism in the slip weakening law formulation, only crack like ruptures may propagate [57]. If strong heterogeneities in the prestress or material properties exist, pulse like ruptures may develop due to the arrest waves sent from these strong heterogeneities [36]. Furthermore, if a pulse like rupture is nucleated in a 2D model using rate dependent friction, it may continue to propagate through regions governed by rate-independent slip weakening friction [58]. However, in general, self-healing pulse like ruptures are not compatible with slip weakening friction.

One observation is that supershear pulses may propagate on uniformly stressed 2D slip weakening faults embedded in a homogeneous medium. These conditions preclude the influence of heterogeneities in the bulk, pre-stress, or friction law. Figure 3.1 shows the space-time evolution of slip rate distribution on the fault for a case with $S = 1$. Initially the rupture propagates in the crack like mode. Through the Burridge-Andrews mechanism, a daughter crack is nucleated ahead of the main rupture tip [See the insert]. This daughter crack propagates in both directions and eventually its rear tip joins the main rupture. However, shortly after this coalescence, the slip rate behind the leading front arrests and a supershear pulse is detached. This pulse propagates intact for the remainder of the simulation time.

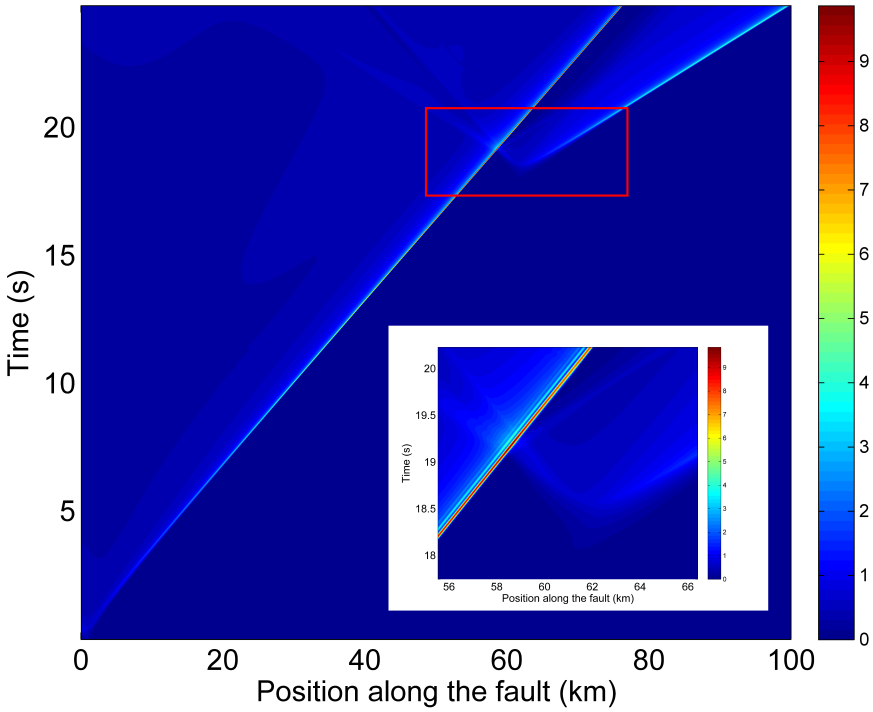

Figure 3.1: Space-time contour of slip rate for homogeneous medium.The nucleation of the daughter crack occurs when the main rupture tip is located at approximately 55 km. Once nucleated, the daughter crack propagates into two directions, and its rear tip joints the main rupture front. A detached supershear rupture is formed shortly after the coalescence.

In Figure 3.2 the slip rate and shear stress distribution are plotted on the fault plane shortly after the supershear pulse detachment. The main rupture continues to propagate in a crack like mode. However, the fault unloads in the vicinity of the trailing edge of the supershear pulse and the shear stress drops below the level of dynamic shear strength (25 MPa). Within the actively slipping regions this does not happen and the shear stress is bounded from below by the minimum strength level specified by the slip weakening law.

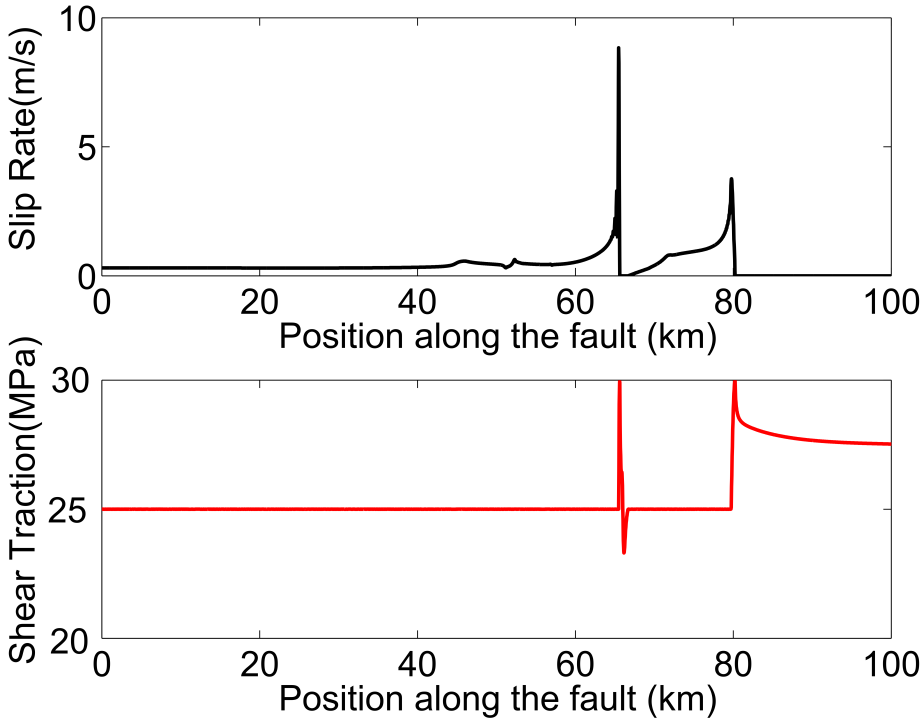

Figure 3.2: Snapshots of slip rate and shear traction on the fault surface after the detachment of the Supershear pulse.The first rupture front represents the Supershear rupture front. Due to the slip rate arrest around 65 to 68 km, the shear traction drops below 25 MPa (The prescribed dynamic frictional stress).

In the absence of heterogeneities, why would a supershear pulse develop? To answer this question the rupture tip driving force is computed [Appendix A]. The rate of change of the driving force is given by:

$$\frac{dF}{dt} = \frac{1}{l}\int_0^l (\tau_o - \tau)\dot{u}dx \tag{3.1}$$

where l is the length of actively slipping region, τ_o is the prestress level,τ is the current value of shear stress, $\dot{u}$ is the slip rate and the integration is taken over the fault surface. The evolution of the rate of change of the driving force is shown in Figure 3.3.

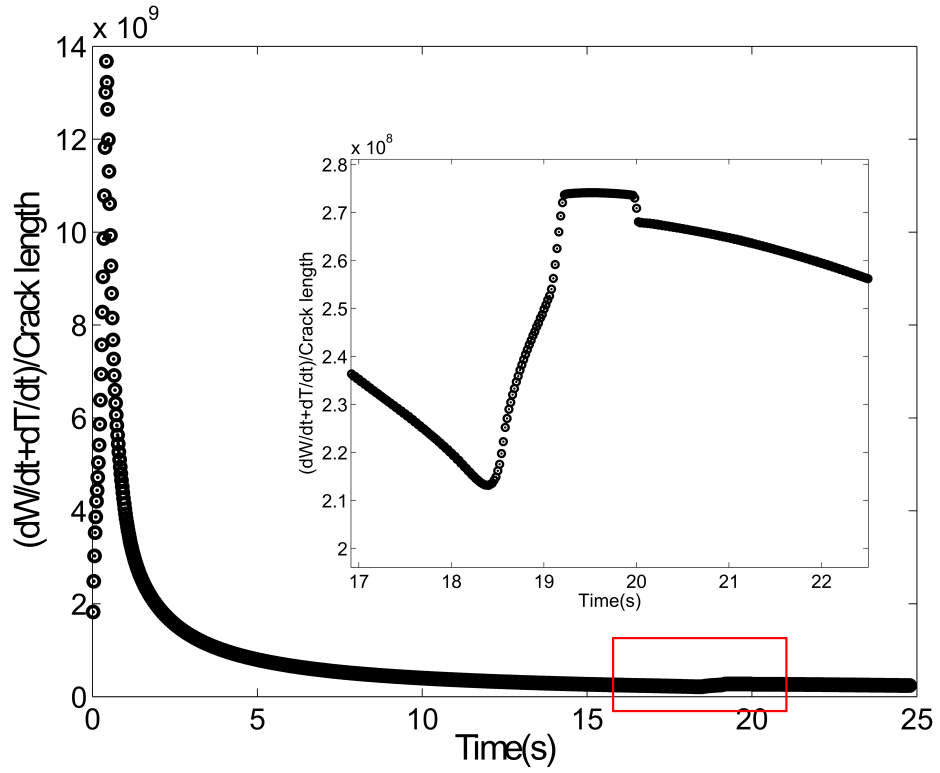

Figure 3.3: Evolution of driving force on the fault surface during the simulation. The jump represents the Supershear occurrence of the nucleation of the daughter crack.The driving force stays constant for some time and then drop due to the detachment of the Supershear pulse.

The abrupt nucleation leads to an initial sharp increase in the crack tip driving force. The rate of change of the force is high in this region. As the crack expands the crack driving force increases but the rate of change of the crack driving force decreases. For a steadily propagating slip pulse the crack driving force is a constant [59]. This corresponds to a propagating rupture with zero change in its driving force. It is hypothesized that cracks are driven towards a similar state with the driving force increases at a progressively decreasing rate as the crack expands. This is probably a more favorable state from the energetic perspective. When the daughter crack nucleates, it

disrupts the pattern and the rate of change of the tip driving force increases. Through the detachment of the slip pulse and the breakdown of the rupture to smaller regions, the rate of change of the driving force decreases again. Hence, it is conjectured that the detachment of the pulse is more favorable because it leads to an overall smaller crack driving force than if the rupture continues to propagate as an intact crack.

3.2 Supershear rupture propagation in the presence of off-fault low velocity inclusion

The existence of an off-fault heterogeneity with a lower shear modulus than the surrounding bulk enriches the wave field by introducing additional boundary surfaces. The waves emanating from the rupture and propagating though the heterogeneous medium are modulated by the reflection and the refraction at the different material interfaces. These modulations include changes in wave amplitudes, phase angles and polarities. In Figure 3.4, the reflection coefficient is plotted for the SV wave at both the lower and upper boundaries of a hypothetical soft layer for the case corresponding to a mismatch in P-wave speed = 20%. Different values of the incidence angle are considered. Waves reflected from the lower boundary of the soft layer have the same polarity as the incident wave for the whole range of incidence angles considered here. Thus, these waves enhance the rupture propagation. On the other hand, the waves reflected from the upper boundary of the soft layer have negative reflection coefficients for incidence angles less than 10°. When these waves are transmitted back to the fault zone, their reversed polarity impedes the rupture and may lead to temporary rupture arrest and formation of slip pulses as will be discussed shortly. This scenario is different from when the low velocity layer is adjacent to the fault plane. In this case, only reflections from the top layer are present leading to rupture decoherence [20, 21].

First consider a fault case with strength parameter $S = 1$. In a homogeneous medium, one observation is that the rupture jumps into supershear after propagating for a distance 55.5 km.

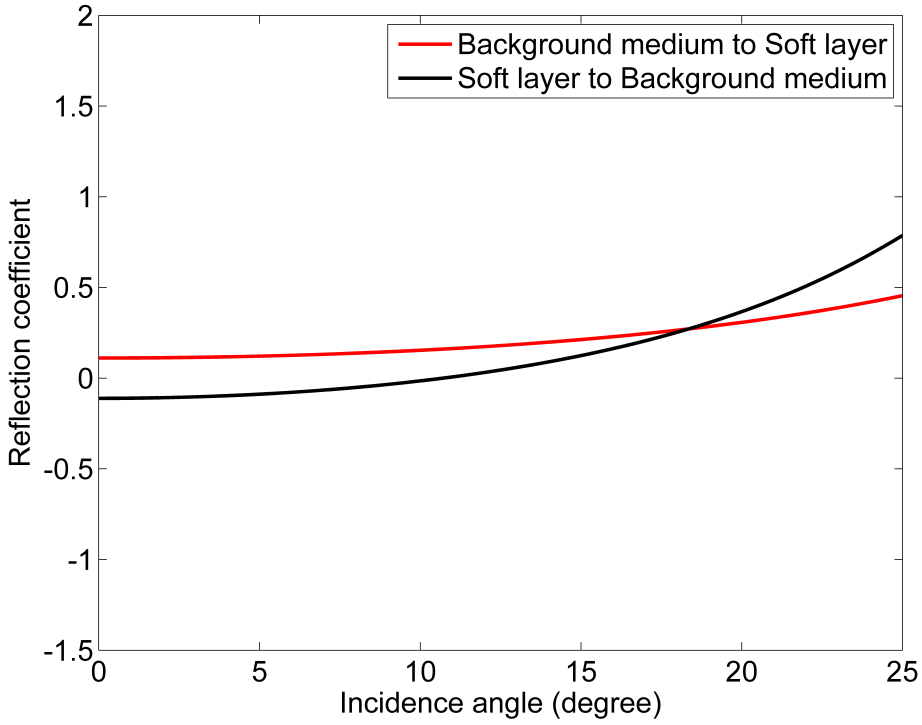

Figure 3.4: Reflection coefficient for incident SV waves at boundary between background medium and soft layer with velocity reduction of 20% ,Red line shows the incident wave background medium to soft layer and black line shows the incident wave from soft layer to background medium respectively.The reflected SV wave is considered.The incident angle of SV waves are plotted below the first critical angel.The phase is zero for this range of incident angels.Formulas of reflection coefficients are taken from [1].

The existence of the soft heterogeneity reduces the supershear transition distance. The extent of the effect depends on many factors such as the soft inclusion thickness, the soft inclusion extension, the soft inclusion distance from the fault and the velocity reduction in the soft inclusion. These factors determine the amplitudes of the waves reflected from the soft layer to the fault zone as well as the perturbations in the nucleation size of the daughter crack. The width of the soft inclusion, in particular, determines the difference in arrival times, as observed on the fault surface, between the different waves reflected from the two boundaries of the soft layer. For a soft inclusion of length 20 km and width $H_2 = 2R$, where R is the nucleation length scale, the transition distance to supershear is reduced to only 15 km compared to more than 55 km for the homogeneous case. This reduction may be attributed to

two reasons. First, the waves reflected from the bottom boundary of the soft inclusion have the same polarity as the incident wave and thus they enhance the rupture propagation. This thickness of the soft inclusion $H_2 = 2R$ is big enough to delay the arrival of the reflected waves from the top boundary. Since these waves have an opposite polarity they interfere destructively with the rupture. When the soft inclusion thickness is smaller (e.g. $H_2 = R$) these waves arrive sooner to the fault surface and compete with the enhanced effect carried by the reflected waves from the bottom boundary. In this case, the transition distance is close to its value in the homogeneous case.

The second reason is that the nucleation length for a crack is proportional to the rigidity of the domain (Eqn. 2.2). The existence of a soft inclusion reduces the effective rigidity of the medium compared to the homogeneous case. Thus the nucleation size of the daughter crack will be smaller in the presence of a soft inclusion. This is shown in Figure 3.5. There, by tracking the width of the region for which the peak shear stress is equal to the static strength, the nucleation size of the daughter crack is defined as the size of this region just before it becomes disjoint. Based on this definition, it is found that the nucleation length of the daughter crack is reduced from 375 m, for the homogeneous medium, to 225 m, for the case with softer inclusion. The nucleation size of the daughter crack is generally smaller than what is predicted for quasi-static nucleation (Eqn. 2.1). This is because the nucleation of the daughter crack is enhanced by the dynamic stress field of the primary crack.

Figure 3.6 shows the variation of the rupture speed for the homogeneous and heterogeneous cases. The method used to compute the rupture speed by recording the location of the rupture tip at each time step. Eliminate numerical artifacts associated with the finite space time discretization by fitting the tip position-time curve with a polynomial of degree 9. By differentiating the smoother curve that resulted from the fitting process, the instantaneous rupture tip speed is computed as shown in Figure 3.6. The shear wave speed as well as the Rayleigh wave speed for the fault zone material are depicted on the same plot.

In both cases, the supershear transition occurs discontinuously through

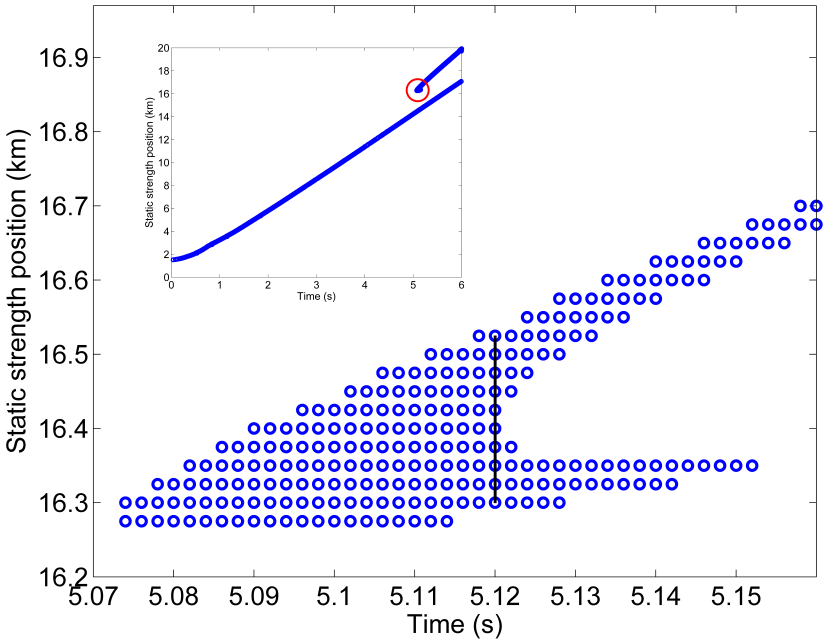

(a)

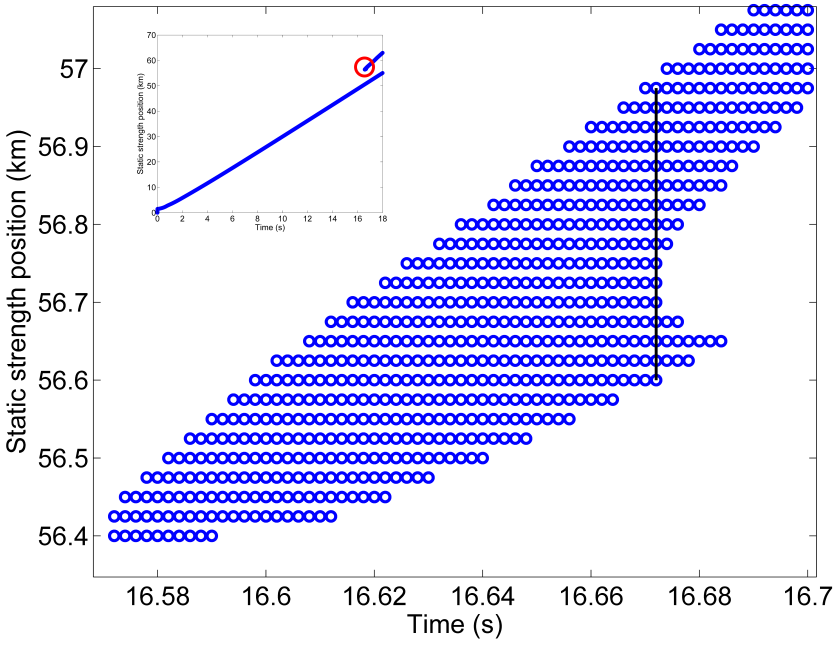

(b)

Figure 3.5: Growth of the daughter crack in the presence (a) and absence (b) of soft inclusion. Here the location of the fault points where the shear stress is equal to the static frictional stress (30 MPa) is plotted. The nucleation length of the daughter crack in the soft layer inclusion case is 225 km while in the homogeneous case is 375 km.

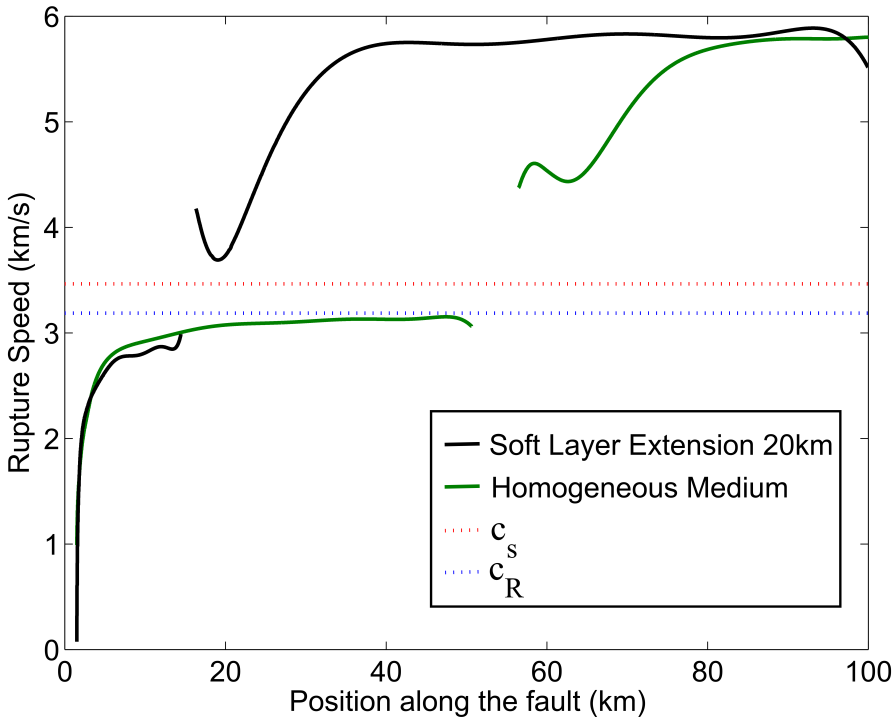

Figure 3.6: Variation of rupture speed for homogeneous medium and medium with soft layer inclusion. The jump represents the nucleation of daughter crack through the Burridge-Andrews mechanism. The dip after the jump represents the mechanism for Supershear rupture to form. The nucleation of daughter crack for homogeneous medium is 55 km, for medium with soft layer inclusion is 15 km.

the nucleation of a daughter crack as predicted by the Burridge-Andrews mechanism. The discontinuity in the rupture speed plot corresponds to the nucleation of the supershear tip. For the homogeneous case, the supershear rupture transition occurs at 55 km whereas for the soft layer case the supershear transition happens at approximately 15 km. In both cases prior to the supershear jump, the rupture travels at sub-Rayleigh wave speed. There is no propagation through the so called 'Energetically Forbidden Zone' defined by the range of velocities between the shear wave and Rayleigh wave speed [60].

Another feature of the rupture speed plot (Figure 3.6) is the existence of a dip shortly after the transition to supershear. This is related to the details of the supershear transition process. Shortly after it is formed, the daugh-

ter crack joins the main rupture and the leading rupture tip propagates at supershear velocity while the main rupture tip is still propagating at lower velocity. As a result the distance between the leading edge and the main rupture front continues to increase leading eventually to the detachment of a supershear pulse. This mechanism occurs in both the homogeneous and layered cases (Figure 3.6). This suggests that the formation of the detached pulse is essentially due to energetic reasons (See Section 3.1) rather than due to the reflections from the soft inclusion. After the detachment, the rupture propagation speed of the slip pulse increases till it saturates at a speed between $\sqrt{2}c_s$ and c_p of the fault zone [31].

Figure 3.7 shows that the space time evolution of the slip rate on the fault surface in the two cases. For the case of homogeneous medium the slip rate is smoother. The multiple reflections from the different interfaces in the medium with a low velocity zone lead to visible oscillations in the slip. These oscillations may become large enough (depending on the material contrast) to lead to the temporary arrest of the rupture behind the leading edge and the formation of a train of pulses (not shown here).

Figure 3.8 shows the evolution of maximum slip rate for both the homogeneous and inhomogeneous media. The existence of the embedded soft inclusion leads to the saturation of the maximum slip rate at 1.2 m/s during the sub-Rayleigh propagation. After the supershear jump, and as the rupture propagates into the homogeneous medium, the maximum slip rate starts to increase again. In the homogeneous case, on the other hand, the maximum slip rate increase monotonically up to 9 m/s in the sub-Rayleigh regime. The sudden jump in the maximum slip rate profile in both cases point to the supershear transition. The end of the drop following this jump refers to the detachment of supershear slip pulse. These observations suggest that the presence of an embedded soft layer inclusion to the occurrence of supershear transition at lower slip than in the homogeneous case. Also the magnitude of the maximum slip rate is smaller in the soft layer case than the homogeneous case even though the rupture propagates faster in the former than in the latter. Same observation applies to the rate of change of the maximum slip rate. Although both tips are propagating in the same homogeneous medium (after the soft inclusion stops), the maximum slip rate increases at a faster

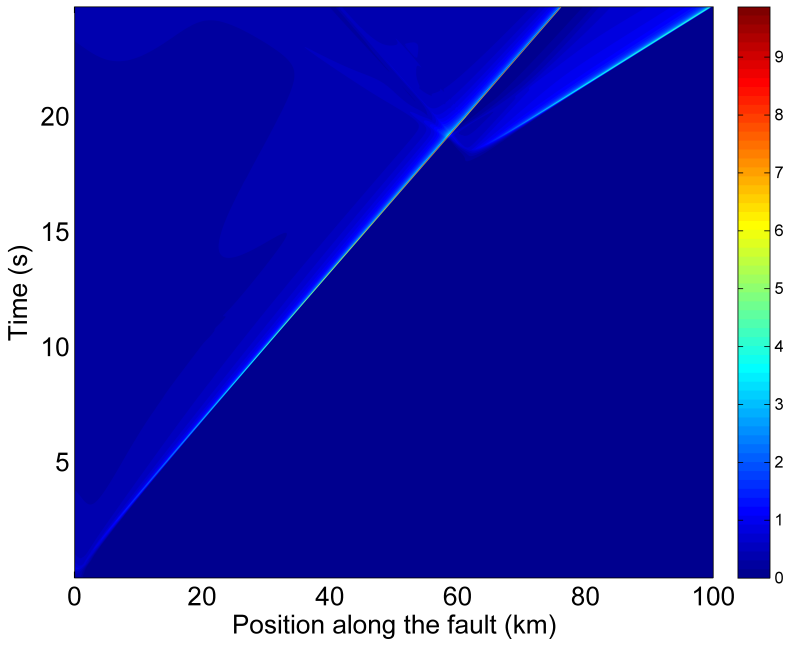

(a)

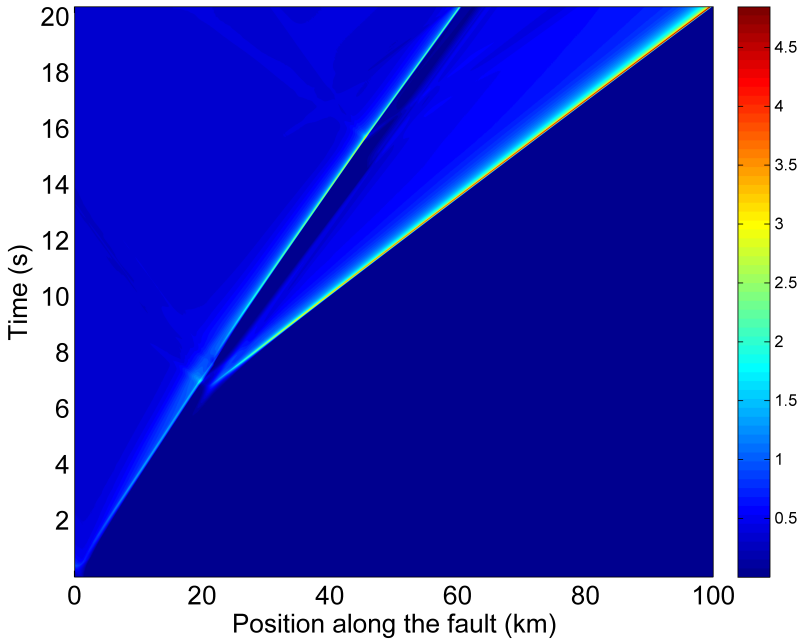

(b)

Figure 3.7: Space-time contours of slip rate on the fault surface (a) homogeneous medium (b) medium with 20km soft layer inclusion.The homogeneous medium has smoother slip rate profile (no oscillations in the slip rate behind the Supershear front).

rate in the homogeneous case than in the case with low velocity lens. This points to the necessity of accounting for the rupture history when estimating rupture quantities such as slip and maximum slip rate

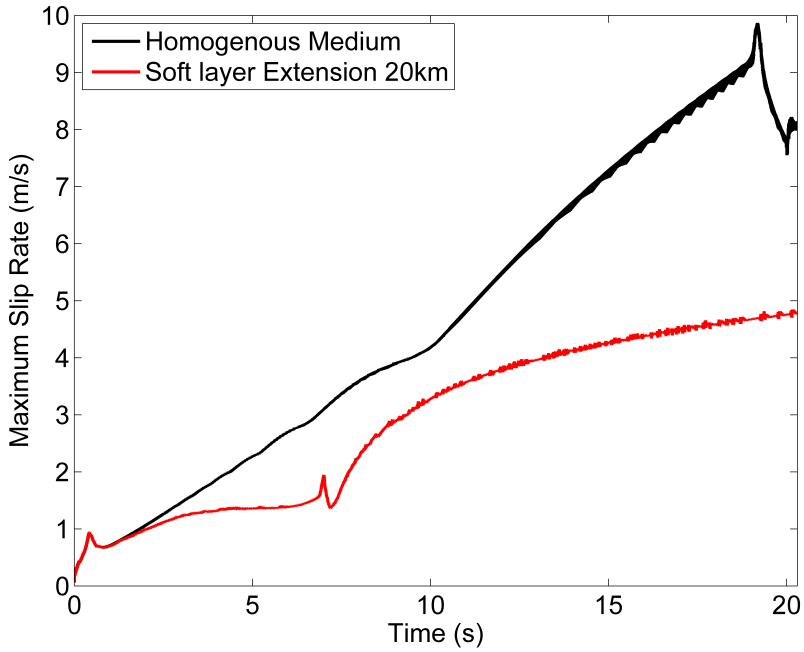

Figure 3.8: Evolution of Maximum Slip rate for homogeneous medium and medium with 20km soft layer inclusion ($H_1 = R$, $H_2 = 2R$, Material Contrast =20%, $L_{nuc} = R$).

In the following sections investigation is carried about the soft inclusion effects in further details. The effect of the soft inclusion thickness, off-fault distance, extension, and material contrast on the supershear transition are explored.

3.3 Effect of Soft inclusion thickness and Off-fault distance

This section investigates the effect of soft layer thickness (H_2) and off-fault distance (H_1) on the supershear transition length. For this purpose, it is assumed that the inclusion extends for the full length of the fault. Normalize these two quantities by R. For $H_2/R = 1$, vary H_1/R between 1 and 8. As

shown in Figure 3.9, the more distant the soft layer is from the fault surface, the longer the transition distance to supershear propagation is. On the other hand, for $H_1/R = 1$, vary H_2/R between 1 and 8. In this case, as the thickness of the soft layer increases, the transition length decreases.

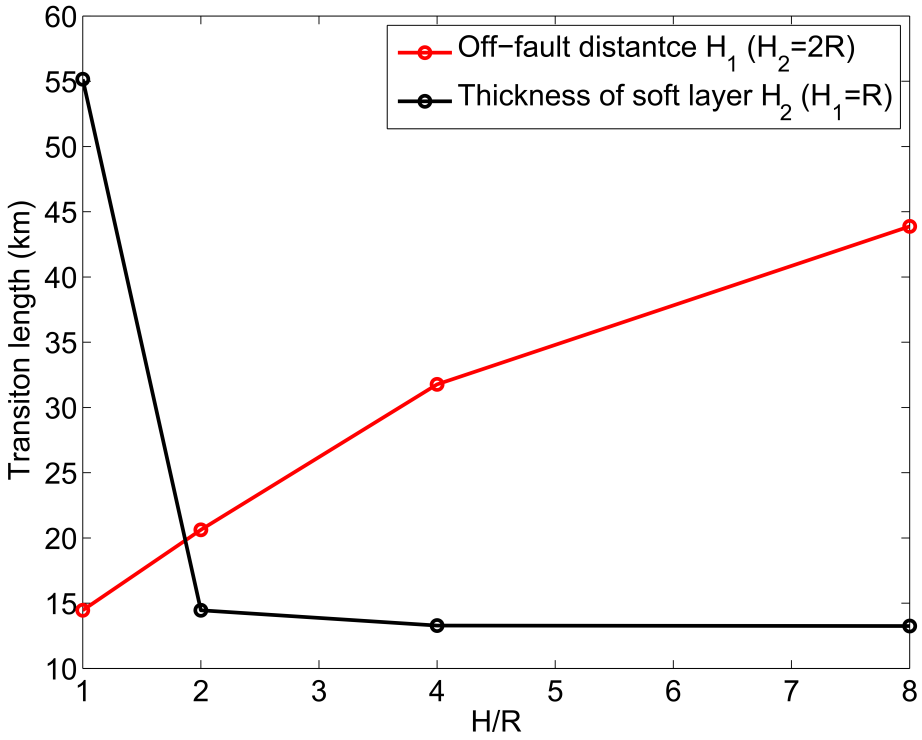

Figure 3.9: Variation of supershear transition length with different values of off-fault distance (H_1) and soft layer thickness (H_2), With $H_2 = 2R$, red line shows transition length to supershear rupture under various off-fault distance H_1. With $H_1 = R$, black line shows transition length to supershear rupture under various soft layer thickness H_2.

These observations are explained as follows. The waves reflected from the top and bottom surfaces of the soft layer have opposite polarities (Figure 3.4). The travel time for a ray emanating from the rupture, reflected from one of these interfaces, and arriving back at the fault surface, depends on the layer thickness as well as its distance from the surface. The more distant the soft layer is from the fault surface, the longer this travel time will be. This has two consequences: (1) there is a delay in the arrival of the waves reflected from the bottom surface. These waves enhance the rupture prop-

agation and accelerate the supershear transition. Their delay, on the other hand, increases the transition length; and (2) the difference in the arrival time between the waves reflected from the two boundaries of the soft layer decreases. In particular, the waves reflected form the upper boundary of the soft layer have reversed polarity and hence they interfere destructively with the propagating rupture as well as with the waves reflected from the bottom boundary delaying the rupture acceleration into supershear.

The increase in the soft layer thickness, on the other hand, enhances the supershear transition and shortens the transition length. This is because as the soft layer thickness increases, the difference in arrival time, as observed at a point on the fault surface, between the waves reflected from the top and bottom boundaries of the soft layer increases. The delayed arrival of the waves reflected from the upper boundary reduces their destructive interference effect (chapter 3.2) allowing more time for the rupture to interact with the waves reflected from the bottom boundary. The latter, having the same polarity as the incident waves, enhances the propagation dynamics and accelerates the rupture transition into supershear. This is shown in Figure 3.9, where the transition length changes significantly as H_2 changes from R to $2R$ but nearly saturates thereafter. This saturation reflects the observation that increasing the soft layer thickness beyond a certain limit is ineffective in changing the transition length. This is because any further delay in the arrival of the reversed polarity waves from the top boundary of the soft layer is irrelevant if the supershear transition has already happened. The trend in Figure 3.9 suggests that variations in the distance of the soft layer from the fault surface have a strong impact on the transition length. On the other hand, the effect of the layer thickness is only relevant for a limited range of thickness values. Increasing the layer thickness beyond a certain value, for a given off-fault distance, has a negligible effect on the supershear transition.

3.4 Effect of Soft layer extension

The low velocity layer may extend to different lengths. It may be an inclusion of a finite extension or a layer extending throughout the full fault length.

Figure 3.10 compares snapshots of slip rate in two cases: (a) a soft layer

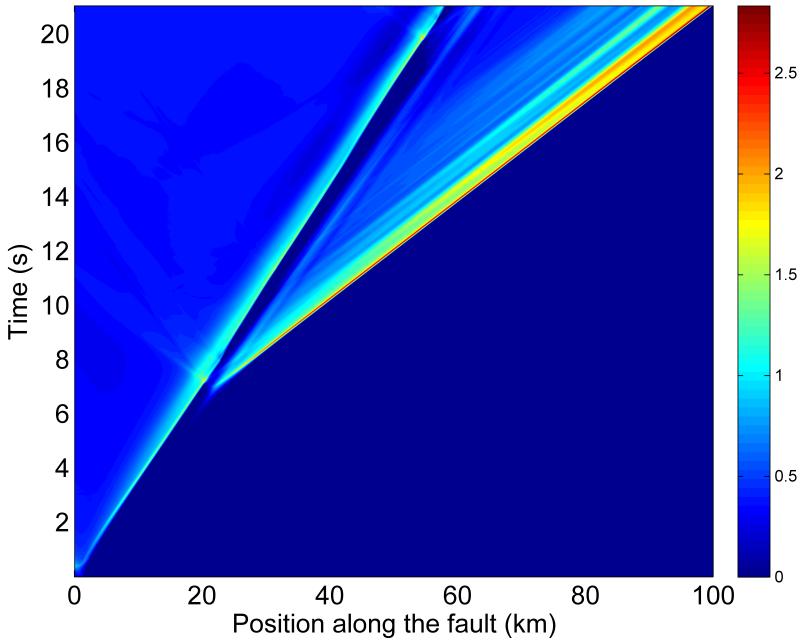

(a)

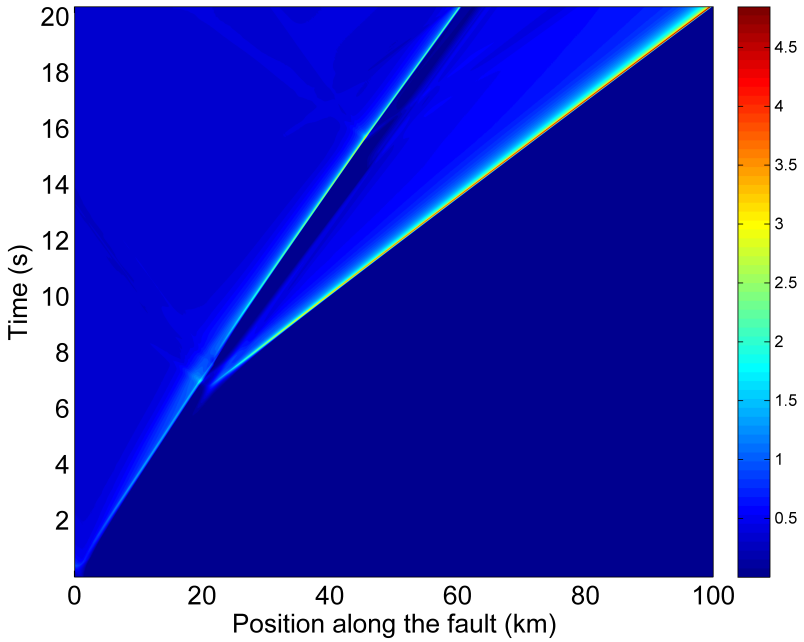

(b)

Figure 3.10: Space-time contour of slip rate during rupture propagations. (a) Soft layer extend to the full length of the domain (100 km) (b) Soft layer extend only 20 km from the left edge of the domain. Case (a) exhibits more oscillations in the slip rate profile behind the supershear rupture front.

extending full length, and (b) a soft layer extending only for 20 km. Both cases have a strength parameter $S = 1$ and the velocity reduction is 20%. For both cases, the supershear transition distance is approximately 15 km. This suggests that accelerated supershear transition is insensitive to the length of the soft layer as long as the length of the soft layer is larger than a critical value. This value is set by the velocity contrast and the distance of the soft layer from the fault surface. Moreover, the rupture continues to propagate as supershear into the homogeneous medium after the truncation of the soft layer at 20 km long. In chapter 4 the implications of this on conditions for accelerated supershear transition under heterogeneous conditions are discussed.

There are, however, a few differences between the two cases. Most notably, the rupture propagating into the homogeneous medium, after the soft layer is truncated, shows a smoother slip rate profile with no oscillations behind the first rupture front. This is not the case when the soft layer extends to the full length of the fault. In this case, the oscillations in the slip rate are caused by the multiple reflections of the waves from the soft layer boundaries. The truncation of the soft layer eliminates the cause of theses oscillations.

In Figure 3.11 compare the rupture speeds for the two cases. Initially, both ruptures have essentially the same rupture speed. However, for the case of the truncated soft layer the rupture speed is slightly higher. This suggests that wave reflections from the upper boundary of the fully extended soft layer interferes destructively with the wave field surrounding the crack tip and slightly lower its propagation speed. These reflections are absent in the case of soft layer extending only for 20 km.

In Figure 3.12 compare the evolution of maximum slip rate when the soft layer has a limited extension of 20 km and when it extends to the full length of the fault. The two cases are identical up to 7 seconds of propagation time. There is a very small difference in the time of supershear transition (see the first peak in the maximum slip rate profile) between the two cases. The supershear transition is slightly delayed in the case of soft layer that is extending for the full length. In this case, wave reflections from the boundaries of the soft layer limit the maximum slip after supershear transition to approximately 2.7 m/s. However, in the case of the 20 km long soft layer,

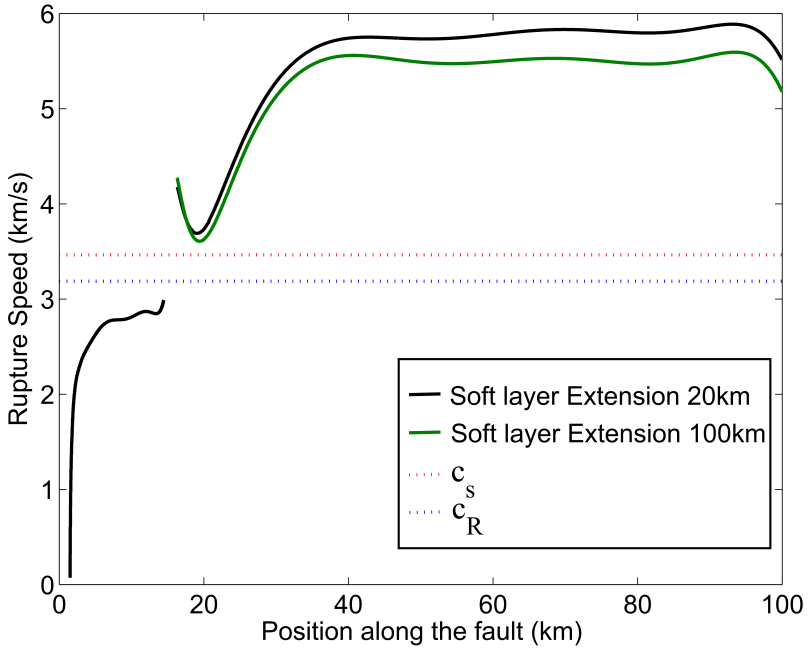

Figure 3.11: Variation of rupture speed for medium with soft layer extending full length and a medium with soft layer only extending 20 km.

the magnitude of the maximum slip rate increases as the rupture propagates into the homogeneous medium.

3.5 Effect of Soft zone position

This section investigates how the position of the soft zone affects the supearshear transition characteristics. Simulations are conducted with soft layer starting from the left edge (i.e. adjacent to the nucleation zone) and extending to only 10 km. The simulation is repeated with the same soft layer length but make it extend from 20 km to 30 km. As it was shown previously [Chapter 3.2], a soft layer extending 20 km from the start of the nucleation site has reduced the transition length to approximately 15 km. For the soft layer starting from the edge and extending 10 km, the supershear transition length (45 km) is slightly reduced compared to the homogeneous case but is much longer than the case with 20 km long soft layer. On the other hand, the transition length corresponding to the shifted soft layer is only 23.4 km. Figure 3.13 shows the space-time evolution of slip rate distribution on the fault for the two cases. The enhanced supershear transition for the case of

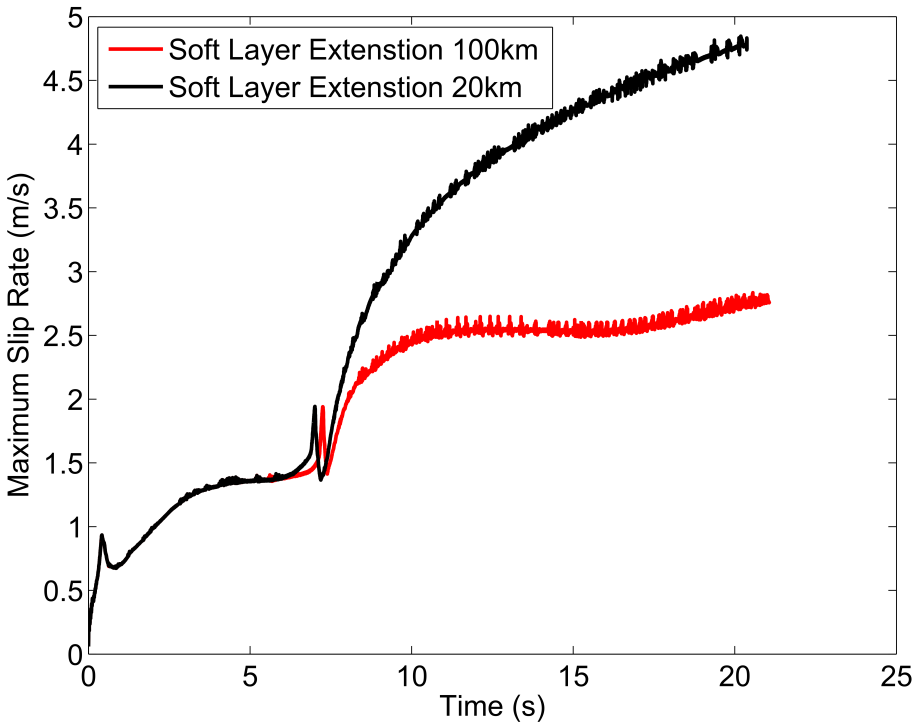

Figure 3.12: Evolution of Maximum Slip rate for soft layer extend 100 km and medium with soft layer extended 30 km.

shifted soft layer may be explained as follows. As the rupture propagates from the left, the S-wave stress peak grows. Waves reflected from the bottom boundary of the shifted layer interfere with the stress peak after the latter has had some time to grow. This interference further strengthens the stress peak and accelerates the transition. This suggests that the same heterogeneity may have different effects on the rupture dynamics depending on its position relative to the spatiotemporal evolution of the crack. If the rupture encounters a favorable off-fault heterogeneity, it will transition faster to supershear. This is similar to the effect of a favorable prestress heterogeneity on the fault surface that was previously discussed by Lapusta and Liu [43].

3.6 Effect of Stress level S ratio and Material contrast

This section investigates the effect of stress level ratio S and material contrast on supershear transition characteristics. The limiting value of strength

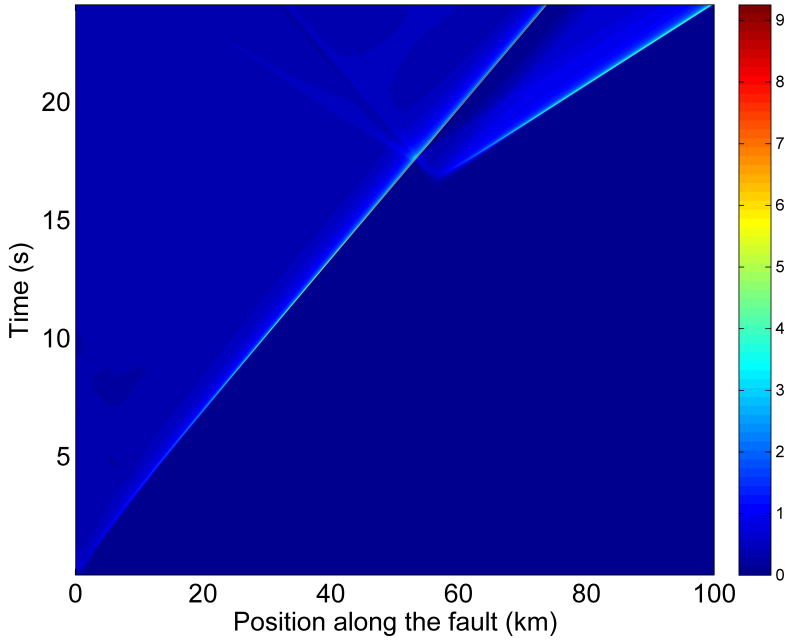

(a)

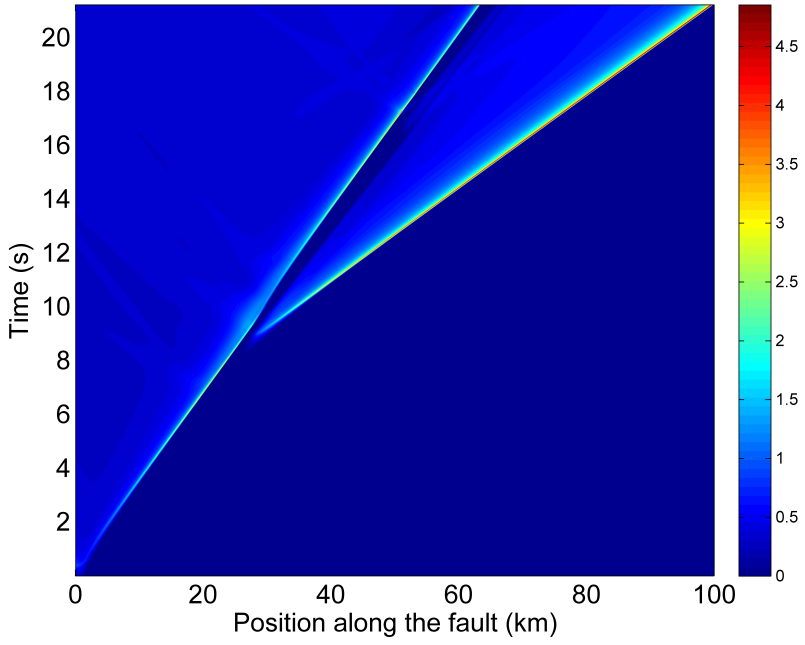

(b)

Figure 3.13: Space-time contours of slip rate (a) soft layer 10 km from beginning (b) soft layer 10 km shifted to 20 to 30 km.

parameter S for supershear rupture to occur in homogeneous 2D elastic media is 1.77. The existence of a soft layer violates the assumption of medium homogeneity and introduces additional interfaces for wave reflection and refraction. In this case, the limiting S value may be different from the homogeneous medium and it may be even non-existent. Indeed, [21] showed that the existence of LVZ adjacent to the fault surface enhances the supershear transition mechanism. Here, a few examples are presented showing that rupture may transition into supershear, or continue to propagate as supershear, under stress values that are lower than the limiting case predicted theoretically for the homogeneous media.

Considering a soft layer that is 20 km long, different prestress distributions are examined. In one case, the value of the strength parameter is $S = 1$ for first 30 km of the fault length and $S = 2$ for the remaining 70 km. One case is also considered with $S = 2.5$ for the last 70 km of the fault length. The choice of the soft layer length and the extent of $S = 1$ regime was to insure that supershear transition will happen within the elevated stress region.

Figure 3.14 shows that the evolution of the rupture speed with respect to the distance along the fault for the two cases just described in addition to a reference case in which $S = 1$ uniformly along the whole fault length. The three cases behave exactly the same before the supershear transition happens This is expected as the rupture conditions are identical in this regime In all cases, the transition distance to supershear is 15 km. After the transition to supershear, the three cases develop a detached supershear slip pulse. This is signaled by the existence of a dip in the rupture speed profile [Please see Chapter 3.1 for further discussion on this]. As the rupture tip approaches the location at which the prestress abruptly changes (30 km), the three cases start to deviate from one another. Waves emitted from the propagating rupture sense variations in the prestress field, even before the rupture tip reaches the lower stress region. Some of these waves are reflected back carrying this information about the reduced prestress to the rupture tip. As a result, the rupture propagation speed decreases for the cases with increased strength parameters. Nonetheless, the difference in the rupture speed after the transition to supershear in all cases is small. Moreover, the rupture continues to propagate supershear even with $S = 2.5$. This suggests that supershear ruptures,

once formed, may persist to propagate in low stress regions that are unfavorable for supershear transition in homogeneous conditions. The existence of off-fault material heterogeneity accelerates the transition to supershear. The supershear propagation may persist thereafter even if the prestress is reduced. The implications of this on supershear transition in understressed faults are discussed in chapter 4.

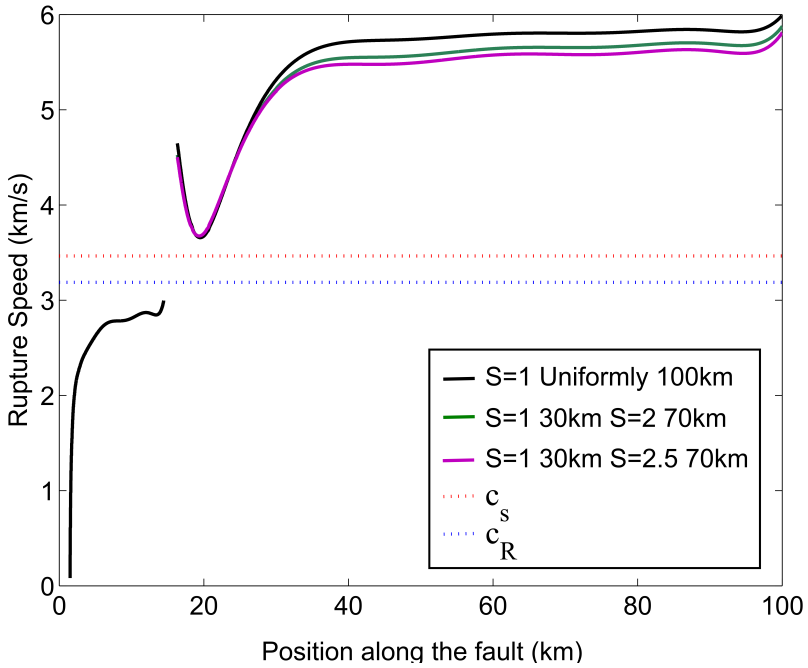

Figure 3.14: Variation of rupture speed for $S = 1$ uniformly 100 km, $S = 1$ for 30 km, $S = 2$ for the rest 70 km and $S = 1$ for 30 km $S = 2.5$ for the rest 70 km. The domain is with 20 km length soft layer inclusion.

The evolution of the maximum slip rate in the three cases is shown in Figure 3.15.The three cases behave exactly the same until the rupture reaches the location of change in the prestress (at 8 seconds). The maximum slip rate, unlike the rupture speed, shows a stronger dependence on the local stress conditions. For the cases of $S = 2$ and $S = 2.5$ the maximum slip rate drops instantaneously in response to the imposed prestress drop. The drop in the maximum slip rate is higher for the case with $S = 2.5$ than for the case with $S = 2.0$.

Investigation is carried out about the possibility of supershear transition

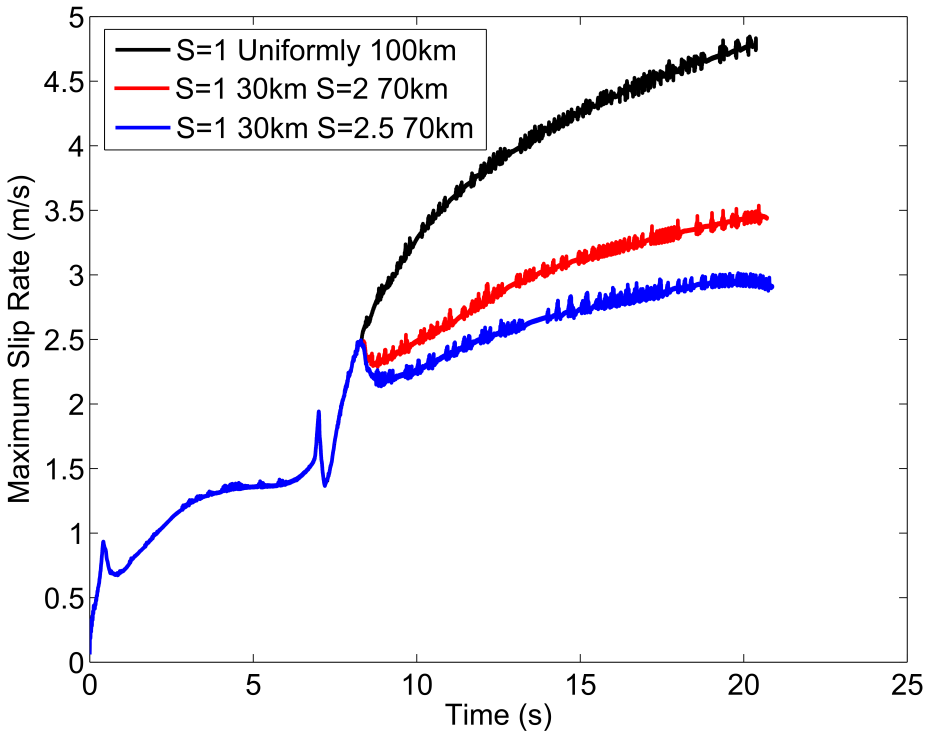

Figure 3.15: Maximum slip rate for $S = 1$ uniformly 100 km, $S = 1$ for 30 km and $S = 2$ for the rest 70 km and $S = 1$ for 30 km $S = 2.5$ for the rest 70 km. The domain is with 20 km length soft layer inclusion.

under uniformly lower prestress levels if the velocity reduction in the soft layer increases. For this purpose simulation is carried out with the soft layer extending parallel to the full length of the fault, considering several values of velocity reduction ranging from 20% to 60%. Figure 3.16 shows that it is possible with higher material contrast to generate supershear ruptures even if the strength parameter is uniform and equal to 2.5 along the fault length. The transition length to supershear propagation increases, however, as the material contrast decreases. For example, one observations is that the supershear transition length, under uniform prestress conditions, is approximately 14 km for the case with material contrast 60% and $S = 2$. This transition length increases to 66 km and 176 km for cases with 40% and 20% velocity reduction in the soft layer respectively. For 0% velocity reduction (homogeneous medium) the transition length is predicted theoretically to be infinite. Thus it is hypothesized that in the presence of an off-fault soft layer, supershear may happen under any stress level but the transition length diverges, for $S > 1.7$, as the material contrast between the soft inclusion and the medium

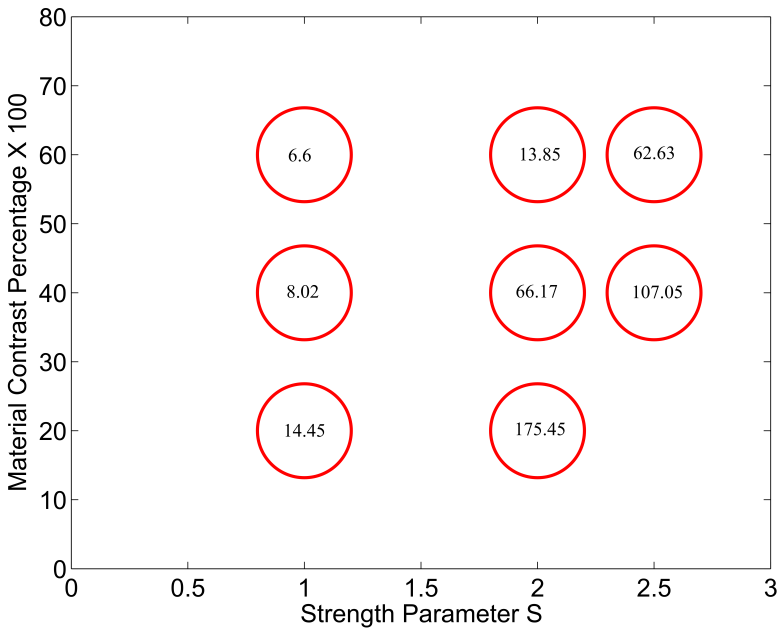

Figure 3.16: Values of Transition length with respect to Material Contrast and Strength Parameter S.

approaches zero. A possible mechanism is that the continuous reflections from the soft layer to the fault surface enhance the building up of the shear stress ahead of the rupture front, and eventually lead to the nucleation of the daughter crack through the Burridge-Andrews mechanism. If the rigidity of the soft layer approaches zero, it may be taken as an analog of a free surface. Supershear transition due to free surface has been investigated for strike slip faults by Kaneko and Lapusta [45]. The observations suggest that supershear transition may occur at low prestress values if a free surface exists parallel to the rupture propagation direction. The implications of this particular observation on rupture propagation on normal fault flats as well as the strike slip faults are discussed in chapter 4.

CHAPTER 4

Discussion

Identifying conditions under which supershear transition may occur during earthquake propagation is crucial for the development of a better understanding of earthquake physics as well as the estimation of ground motions. Supershear ruptures tend to be more destructive since the resulting waves travel longer distances with less attenuation than in their sub-shear counterparts [31]. Heterogeneities in the Earth's crust are manifested in different forms. These include heterogeneities in the prestress, material properties and friction laws. Exploring the interplay between different sources of heterogeneities and the dynamics of the rupture process is essential for the development of more realistic rupture models.

In this paper, the influence of the existence of an off-fault material heterogeneity is explored, represented by an off-fault low velocity lens, on the rupture dynamics on a slip weakening frictional interface. The primary focus is on its effects on transition to supershear. Previous studies focused on other sources of heterogeneities such as variations in the prestress [43] or fracture energy [61]. The investigation is similar to Harris and Day [18], Huang and Ampuero [20], and [21], where the authors explored the influence of a low velocity zone adjacent to the fault surface. A point of departure for the approach in this paper is for allowing the low velocity layer to be placed at a finite distance from the fault surface. Moreover, the low velocity zone may be present in the form of a velocity anomaly within a limited region and need not extend throughout the length of the domain.

Velocity structure in the upper crust is generally heterogeneous [2]. It is most natural to think of low velocity zones to be present in the immediate vicinity of pre-existing faults as a result of the damage caused by previous earthquakes. However, there may be situations in which the low velocity zone

exists near but not immediately adjacent to the fault surface. Examples include (i) faults in the shallow parts of the crust near sedimentary basins, (ii) a member of a fault network in which the damaged zone adjacent to a nearby fault has lower rigidity than the damage zone in its immediate vicinity. Moreover, recent developments in the unified velocity structure models [2] show that spatially heterogeneous velocity structure is more common than what was originally thought of. With increased resolution and better detection methods, capability to identify more fine scale variations in this heterogeneous structure will be achieved.

Different friction models have been developed to describe the evolution of fault strength. These include the slip weakening models [53, 54, 56], the rate and state friction [62, 63], and the shear transformation zone theory [64, 65, 66, 67]. Rate dependent models such as the Deterich-Ruina formulation or STZ friction models capture the evolution in fault strength in response to velocity changes and naturally accounts for healing as the slip rate is reduced. These features have important implications for rupture mode classification [68, 69]. Linear slip weakening models, on the other hand, do not naturally allow for fault healing and are insensitive to rate effects. Nonetheless, it is possible to map the parameters of slip weakening friction to the corresponding parameters in the logarithmic rate and state law [43]. Thus, the results of the current study, derived based on linear slip weakening friction, are expected to hold, at least qualitatively, if a more sophisticated logarithmic rate and state description is used.

The dynamic friction used in this study is equal to 0.5. This leads to a reasonable value of static stress drop (25 MPa) [70]. However, this is relatively high compared to the expected strength level for mature faults. Due to the heat flow anomaly and lack of evidence for melting on mature faults [71, 72, 73], the actual value for dynamic friction is expected to be as low as 0.1 or 0.2. Several mechanisms have been proposed to account for the ultra-low dynamic friction including flash heating [73, 74], pore fluid pressurization [73, 75], silica gel formation [73] and nanoparticle lubrication [76]. Thus it is expected that the heat generation associated with the friction model used in the paper to be high and possibly consistent only with slip on dry and less mature faults [77] where traces of pseudotachylytes have been documented.

Appreciate, however, that the rapid transition from high static friction to low dynamic friction is important for enabling rupture propagation in relatively low prestress conditions [78]. The details of this transition has direct implications for the rupture mode classification and generation of self-healing slip pulses [57, 79]. Extend this study to account for strong rate weakening friction will be made in future investigations.

Slip pulses have been observed in dynamic rupture simulations under different conditions. These include models with strong rate weakening friction [68], strong material or prestress heterogeneities [36], low velocity zones [20], and heterogeneous friction conditions [58]. Here, one observationis that it is possible to generate a sustained slip pulse on a slip weakening fault within a homogeneous elastic medium as a consequence of the supershear transition. It is hypothesized that the detachment of the supershear pulse in this case is more favorable from an energetic point of view as it enables rupture propagation with a smaller crack tip driving force. A similar observation of supershear slip pulse was made by Festa and Villote [39] who investigated the influence of nucleation procedure on supershear transition.

In this study the nucleation of the rupture abruptly is carried by overstressing a region of the fault beyond its static frictional strength. This artificial nucleation leads to the rupture propagating dynamically from the beginning. This is different from the more natural quasi-static nucleation of real earthquakes. However, it is not rare that an earthquake may be triggered dynamically due by waves emitted from another earthquake [80, 81, 82]. In this case the nucleation will not be quasi-static. Moreover, this procedure is routinely used in generating laboratory earthquakes [83]. Different nucleation protocols may affect the subsequent rupture propagation. In this paper, the same nucleation procedure as well as the same nucleation parameters are used in all the simulations. Thus the artifacts that may be produced by the abrupt rupture initiation is common to all the results and any observed variations may be attributed to changes in the other model parameters such as the soft layer thickness, or off-fault distance, or material contrast.

The operation of most mature faults under overall low prestress [78] poses a paradox for supershear ruptures. On one hand, analytical and computational

models predict that a relatively high prestress value ($S < 1.77$) is required for supershear transition to occur within a finite distance on slip weakening frictional faults in 2D homogenous elastic media [40]. Meanwhile, if supershear rupture propagation occurs on a mature fault it must then occur at a much lower prestress. A possible resolution to this paradox include the existence of favorable heterogeneities in the fault prestress [43], heterogeneities in the fracture energy [40], or the existence of low velocity zone adjacent to rate and state frictional fault [21]. Here, an additional mechanism which is the existence of off-fault soft heterogeneities is presented. The reflection of waves from the bottom boundary of the off-fault low velocity region enhances the supershear transition and leads to the building up of stresses ahead of the rupture tip at a much lower background stress. One observations is that as the velocity contrast between the inclusion and the background medium increases, the transition to supershear decreases. Moreover supershear propagation at prestress values corresponding to $S > 1.77$ is observed. This may suggest that the velocity structure near the fault surface plays an important role in determining the rupture propagation speed. Accounting for these heterogeneities will give more insight into conditions for supershear transition beyond what is possible from homogeneous models or heterogeneities limited to the fault surface only.

If the elastic moduli of the soft layer are taken to zero in the limit, the soft layer bottom boundary will approach the free surface condition. One observation is that the transition length decreases as the material contrast between the soft layer and the background layer increases. Moreover, as the material contrast increases, the prestress value at which supershear propagation becomes possible decreases. The existence of a free surface parallel to the rupture strike may enable supershear transition at much lower prestress values than what is predicted for the full space case. This situation is relevant to rupture propagation along flat portions in normal faults as well as propagation along the strike of subduction zones. Investigation on this topic further is planned in future studies.

Future extension of this study may include the consideration of more realistic friction constitutive models such as rate and state friction with enhanced coseismic weakening, modeling the existence of off-fault stiff inclusions, and

representing more complex off-fault velocity structure. These investigations will also have implications for engineered composite materials in which the heterogeneous structure modulates the effective fracture toughness [84].

CHAPTER 5

Conclusion

Analysis is conducted about the supershear transition induced by an off-fault low velocity zone using simulations of spontaneous dynamic rupture on a fault governed by a linear slip-weakening friction law embedded in 2D elastic medium. Analysis is carried out about factors that control the transition length to supershear rupture including the thickness of the soft layer, the contrast in the wave velocity between the soft inclusion and the rest of the domain, the stress level on the fault and the length and position of the soft layer. The conclusions are:

1. For the same prestress value, the transition to supershear rupture may occur at much smaller distances due to the existence of the soft layer.

2. For the same material contrast, the transition length decreases with the increase of the soft layer thickness (at a fixed off-fault distance) but increases with the increase of the distance between the layer and fault plane (at a fixed soft layer thickness).

3. The maximum reduction in the transition length happens if the soft layer extends to a distance that is slightly larger than the transition length value predicted for a soft layer that has the same length as the fault. That is, the extension of the soft layer beyond this value has a negligible effect on the transition length.

4. Supershear propogation may happen at a much low prestress in the existence of an off-fault soft layer. The transition length, however, increases as the velocity contrast between the soft layer and the medium decreases.

APPENDIX A

Driving Force Derivation

Start with the equation of motion of a body in R^3

$$\rho \ddot{u} = \nabla \cdot \sigma \tag{A.1}$$

Multiply both sides by the particle velocity and integrate over the whole volume to get:

$$\begin{aligned} \int_V \rho \ddot{u}_i \dot{u}_i dV &= \int_V \sigma_{ij,j} u_i dV \\ &= \int_V (\sigma_{ij} \dot{u}_i)_{,j} dV - \int_V \sigma_{ij} \dot{u}_{i,j} dV \\ &= \int_{C+\Gamma} \sigma_{ij} \dot{u}_i n_j dV - \int_V \sigma_{ij} \dot{u}_{i,j} dV \end{aligned} \tag{A.2}$$

Where V is the volume of the continuum body bounded in the far field by a contour C and includes a surface of discontinuity within it that is covered by the contour Γ as shown in Figure A.1

Rearranging terms:

$$\int_V \rho \ddot{u}_i \dot{u}_i dV + \int_V \sigma_{ij} \dot{u}_{i,j} dV - \int_C \sigma_{ij} \dot{u}_i n_j dV = \int_\Gamma \sigma_{ij} \dot{u}_i n_j dV \tag{A.3}$$

But the total stress is the sum of the initial stress and the elastic stress change:

$$\sigma_{ij} = \sigma^o_{ij} + C_{ijkl} u_{k,l} \tag{A.4}$$

Moreover by using Reynolds transport theorem the rate of change of kinetic

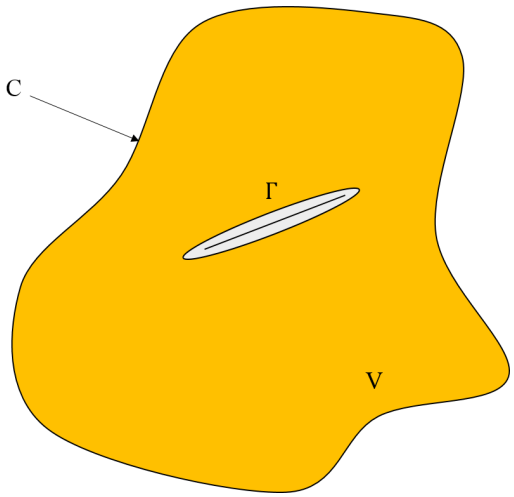

Figure A.1: Arbitrary Domain V with an embedded fault surface . The domain V is bounded by contour C.

energy (T) can be written as:

$$\frac{dT}{dt} = \frac{d}{dt}\int\limits_V \frac{1}{2}\rho \dot{u}_i \dot{u}_i dV = \int\limits_V \rho \ddot{u}_i \dot{u}_i dV + \int\limits_\Gamma \frac{1}{2}\rho \dot{u}_i \dot{u}_i v_r n_j dS \tag{A.5}$$

Where the surface integral is taken only along Γ since C is fixed in space and large enough to include the whole fault. Here v is the velocity by which the contour Γ is moving and n is the normal to contour surface. The normality condition cancels the contribution of the last term in (A.5) for an in-plane shear rupture. Hence drop this term out in the subsequent discussion (If allowing for crack opening then this term will assume nonzero value)

Similarly the rate of change of strain energy (w) can be found from:

$$\begin{aligned}
\int\limits_V \sigma_{ij}\dot{u}_{i,j} dV &= \int\limits_V \sigma^o_{ij}\dot{u}_{i,j} dV + \int\limits_V C_{ijkl} u_{k,l}\dot{u}_{i,j} dV \\
&= \int\limits_V \sigma^o_{ij}\dot{u}_{i,j} dV + \frac{d}{dt}\frac{1}{2}\int\limits_V C_{ijkl} u_{k,l}\dot{u}_{i,j} dV \\
&= \int\limits_V \sigma^o_{ij}\dot{u}_{i,j} dV + \frac{dw}{dt}
\end{aligned} \tag{A.6}$$

Arriving at the following Power Identify by combining all the above:

$$\frac{dT}{dt} + \frac{dw}{dt} - \int_C \sigma_{ij}\dot{u}_i n_j dS = \int_\Gamma (\sigma_{ij} - \sigma^o_{ij})\dot{u}_i n_j d\Gamma \tag{A.7}$$

Recognize that the contour integral over the far fixed contour C as the rate of change of energy radiation, if C is taken far enough then its contribution to the energy balance during rupture propagation is zero. In this case the energy balance reduces to:

$$\frac{dT}{dt} + \frac{dw}{dt} = \int_\Gamma (\sigma_{ij} - \sigma^o_{ij})\dot{u}_i n_j d\Gamma \tag{A.8}$$

Where

$$T = \frac{1}{2}\int_V \rho \dot{u}_i \dot{u}_i dV \tag{A.9}$$

Is the kinetic energy and

$$w = \frac{1}{2}\int_V C_{ijkl} u_{k,l} u_{i,j} dV \tag{A.10}$$

Is the strain energy for a linearly elastic solid.

In 2D domain the discontinuous surface will reduce to a line, and rate of change of the driving force is given by the following formula:

$$\frac{dF}{dt} = \frac{1}{l}\int_0^l (\tau_o - \tau)\dot{u} dx \tag{A.11}$$

In (A.11) the work rate integral was normalized by l which is the instantaneous crack length.

REFERENCES

[1] K. Aki and P. G. Richards, *Quantitative Seismology.* Univ. Sci.Books, Sausalito, Calif, 2002.

[2] Southern California Earthquake Center Caltech.Dataset, 2013.

[3] Y. B. Zion and C. G. Sammis, "Characterization of fault zones," *Pure and Applied Geophysics*, vol. 160, no. 3-4, pp. 677–715, 2003.

[4] Y. G. Li and P. C. Leary, "Fault zone trapped seismic waves," *Bulletin of the Seismological Society of America*, vol. 80, no. 5, pp. 1245–1271, October 01 1990.

[5] Y. G. Li, P. Chen, E. S. Cochran, J. E. Vidale, and T. Burdette, "Seismic evidence for rock damage and healing on the san andreas fault associated with the 2004 m 6.0 parkfield earthquake," *Bulletin of the Seismological Society of America*, vol. 96, no. 4B, pp. S349–S363, September 01 2006.

[6] M. A. Lewis and Y. Ben-Zion, "Diversity of fault zone damage and trapping structures in the parkfield section of the san andreas fault from comprehensive analysis of near fault seismograms," *Geophysical Journal International*, vol. 183, no. 3, pp. 1579–1595, December 01 2010.

[7] M. A. Lewis, Z. Peng, Y. Ben-Zion, and F. L. Vernon, "Shallow seismic trapping structure in the san jacinto fault zone near anza, california," *Geophysical Journal International*, vol. 162, no. 3, pp. 867–881, September 01 2005.

[8] H. Yang and L. Zhu, "Shallow low-velocity zone of the san jacinto fault from local earthquake waveform modelling," *Geophysical Journal International*, vol. 183, no. 1, pp. 421–432, October 01 2010.

[9] Y. G. Li, K. Aki, D. Adams, A. Hasemi, and W. H. K. Lee, "Seismic guided waves trapped in the fault zone of the landers, california, earthquake of 1992," *Journal of Geophysical Research: Solid Earth*, vol. 99, no. B6, pp. 11 705–11 722, 1994.

[10] Z. Peng, Y. Ben-Zion, A. J. Michael, and L. Zhu, "Quantitative analysis of seismic fault zone waves in the rupture zone of the 1992 landers, california, earthquake: evidence for a shallow trapping structure," *Geophysical Journal International*, vol. 155, no. 3, pp. 1021–1041, December 01 2003.

[11] H. Li, L. Zhu, and H. Yang, "High-resolution structures of the landers fault zone inferred from aftershock waveform data," *Geophysical Journal International*, vol. 171, no. 3, pp. 1295–1307, December 01 2007.

[12] Y. G. Li, J. E. Vidale, S. M. Day, D. D. Oglesby, and the SCEC Field Working Team, "Study of the 1999 m 7.1 hector mine, california, earthquake fault plane by trapped waves," *Bulletin of the Seismological Society of America*, vol. 92, no. 4, pp. 1318–1332, May 01 2002.

[13] E. S. Cochran, Y. G. Li, P. M. Shearer, S. Barbot, Y. Fialko, and J. E. Vidale, "Seismic and geodetic evidence for extensive, long-lived fault damage zones," *Geology*, vol. 37, no. 4, pp. 315–318, April 01 2009.

[14] H. Yang, L. Zhu, and E. S. Cochran, "Seismic structures of the calico fault zone inferred from local earthquake travel time modelling," *Geophysical Journal International*, vol. 186, no. 2, pp. 760–770, August 01 2011.

[15] T. Mizuno, Y. Kuwahara, H. Ito, and K. Nishigami, "Spatial variations in fault-zone structure along the nojima fault, central japan, as inferred from borehole observations of fault-zone trapped waves," *Bulletin of the Seismological Society of America*, vol. 98, no. 2, pp. 558–570, April 01 2008.

[16] Y. Ben-Zion, Z. Peng, D. Okaya, L. Seeber, J. G. Armbruster, N. Ozer, A. J. Michael, S. Baris, and M. Aktar, "A shallow fault-zone structure illuminated by trapped waves in the karadereduzce branch of the north anatolian fault, western turkey," *Geophysical Journal International*, vol. 152, no. 3, pp. 699–717, March 01 2003.

[17] R. J. Archuleta and S. M. Day, "Dynamic rupture in a layered medium: The 1966 parkfield earthquake," *Bulletin of the Seismological Society of America*, vol. 70, no. 3, pp. 671–689, June 01 1980.

[18] R. A. Harris and S. M. Day, "Effects of a low-velocity zone on a dynamic rupture," *Bulletin of the Seismological Society of America*, vol. 87, no. 5, pp. 1267–1280, October 01 1997.

[19] Y. Ben-Zion and Y. Huang, "Dynamic rupture on an interface between a compliant fault zone layer and a stiffer surrounding solid," *Journal of Geophysical Research: Solid Earth*, vol. 107, no. B2, pp. ESE 6–1–ESE 6–13, 2002.

[20] Y. Huang and J. P. Ampuero, "Pulse-like ruptures induced by low-velocity fault zones," *Journal of Geophysical Research: Solid Earth*, vol. 116, no. B12, pp. – B12 307, 2011.

[21] Y. Huang, J. P. Ampuero, and D. V. Helmberger, "Earthquake ruptures modulated by waves in damaged fault zones," *Journal of Geophysical Research: Solid Earth*, vol. 119, no. 4, pp. – 2013JB010 724, 2014.

[22] R. J. Archuleta, "A faulting model for the 1979 imperial valley earthquake," *Journal of Geophysical Research: Solid Earth*, vol. 89, no. B6, pp. 4559–4585, 1984.

[23] P. Spudich and E. Cranswick, "Direct observation of rupture propagation during the 1979 imperial valley earthquake using a short baseline accelerometer array," *Bulletin of the Seismological Society of America*, vol. 74, no. 6, pp. 2083–2114, December 01 1984.

[24] M. Bouchon, N. Toksz, H. Karabulut, M.-P. Bouin, M. Dietrich, M. Aktar, and M. Edie, "Seismic imaging of the 1999 izmit (turkey) rupture inferred from the near-fault recordings," *Geophysical Research Letters*, vol. 27, no. 18, pp. 3013–3016, 2000.

[25] M. Bouchon, M.-P. Bouin, H. Karabulut, M. N. Toksz, M. Dietrich, and A. J. Rosakis, "How fast is rupture during an earthquake? new insights from the 1999 turkey earthquakes," *Geophysical Research Letters*, vol. 28, no. 14, pp. 2723–2726, 2001.

[26] A. O. Konca, S. Leprince, J.-P. Avouac, and D. V. Helmberger, "Rupture process of the 1999 mw 7.1 duzce earthquake from joint analysis of spot, gps, insar, strong-motion, and teleseismic data: A supershear rupture with variable rupture velocity," *Bulletin of the Seismological Society of America*, vol. 100, no. 1, pp. 267–288, February 01 2010.

[27] M. Bouchon and M. Valle, "Observation of long supershear rupture during the magnitude 8.1 kunlunshan earthquake," *Science*, vol. 301, no. 5634, pp. 824–826, August 08 2003.

[28] D. P. Robinson, C. Brough, and S. Das, "The mw 7.8, 2001 kunlunshan earthquake: Extreme rupture speed variability and effect of fault geometry," *Journal of Geophysical Research: Solid Earth*, vol. 111, no. B8, pp. – B08 303, 2006.

[29] M. Valle, M. Lands, N. M. Shapiro, and Y. Klinger, "The 14 november 2001 kokoxili (tibet) earthquake: High-frequency seismic radiation originating from the transitions between sub-rayleigh and supershear rupture velocity regimes," *Journal of Geophysical Research: Solid Earth*, vol. 113, no. B7, pp. – B07 305, 2008.

[30] K. T. Walker and P. M. Shearer, "Illuminating the near-sonic rupture velocities of the intracontinental kokoxili mw 7.8 and denali fault mw 7.9 strike-slip earthquakes with global p wave back projection imaging," *Journal of Geophysical Research: Solid Earth*, vol. 114, no. B2, pp. – B02 304, 2009.

[31] E. M. Dunham and R. J. Archuleta, "Evidence for a supershear transient during the 2002 denali fault earthquake," *Bulletin of the Seismological Society of America*, vol. 94, no. 6B, pp. S256–S268, December 01 2004.

[32] M. Celebi, R. Kayen, W. L. Ellsworth, J. R. Evans, E. G. Jensen, M. C. Metz, D. J. Nyman, J. W. Roddick, P. Spudich, and C. D. Stephens, "Near-field ground motion of the 2002 denali fault, alaska, earthquake recorded at pump station 10," *Earthquake Spectra*, vol. 20, no. 3, pp. 597–615, 2004.

[33] R. Burridge, "Admissible speeds for plane-strain self-similar shear cracks with friction but lacking cohesion," pp. 439–455, December 01 1973.

[34] D. J. Andrews, "Rupture velocity of plane strain shear cracks," *Journal of Geophysical Research*, vol. 81, no. 32, pp. 5679–5687, 1976.

[35] S. DAS and K. AKI, "A numerical study of two-dimensional spontaneous rupture propagation," *Geophysical journal international*, vol. 50, no. 3, pp. 643–668, 1977.

[36] S. DAY, "3-dimensional simulation of spontaneous rupture - the effect of nonuniform prestress," *Bulletin of the Seismological Society of America*, vol. 72, no. 6, pp. 1881–1902, 1982.

[37] R. Madariaga and K. B. Olsen, "Criticality of rupture dynamics in 3-d," *Pure and Applied Geophysics*, vol. 157, no. 11-12, pp. 1981–2001, 2000.

[38] E. Fukuyama and K. B. Olsen, "A condition for super-shear rupture propagation in a heterogeneous stress field," *Pure and Applied Geophysics*, vol. 159, no. 9, pp. 2047–2056, 2002.

[39] G. Festa and J. P. Vilotte, "Influence of the rupture initiation on the intersonic transition: Crack-like versus pulse-like modes," *Geophysical Research Letters*, vol. 33, no. 15, pp. – L15 320, 2006.

[40] E. M. Dunham, "Conditions governing the occurrence of supershear ruptures under slip-weakening friction," *Journal of Geophysical Research: Solid Earth*, vol. 112, no. B7, pp. – B07 302, 2007.

[41] Y. Liu and N. Lapusta, "Transition of mode ii cracks from sub-rayleigh to intersonic speeds in the presence of favorable heterogeneity," *Journal of the Mechanics and Physics of Solids*, vol. 56, no. 1, pp. 25–50, 1 2008.

[42] Z. Shi, Y. B. Zion, A. Needleman, and Y. BENZION, "Properties of dynamic rupture and energy partition in a solid with a frictional interface," *Journal of the Mechanics and Physics of Solids*, vol. 56, no. 1, pp. 5–24, 2008.

[43] N. Lapusta and Y. Liu, "Three-dimensional boundary integral modeling of spontaneous earthquake sequences and aseismic slip," *Journal of geophysical research*, vol. 114, no. B9, 2009.

[44] E. G. Daub, M. L. Manning, and J. M. Carlson, "Pulse-like, crack-like, and supershear earthquake ruptures with shear strain localization," *Journal of Geophysical Research: Solid Earth*, vol. 115, no. B5, pp. – B05 311, 2010.

[45] Y. Kaneko and N. Lapusta, "Supershear transition due to a free surface in 3-d simulations of spontaneous dynamic rupture on vertical strike-slip faults," *Tectonophysics*, vol. 493, no. 34, pp. 272–284, 10/18 2010.

[46] S. Langer, L. Olsen-Kettle, and D. Weatherley, "Identification of supershear transition mechanisms due to material contrast at bimaterial faults," *Geophysical Journal International*, vol. 190, no. 2, pp. 1169–1180, August 01 2012.

[47] A. A. Gabriel, J. P. Ampuero, L. A. Dalguer, and P. M. Mai, "The transition of dynamic rupture styles in elastic media under velocity-weakening friction," *Journal of Geophysical Research: Solid Earth*, vol. 117, no. B9, pp. – B09 311, 2012.

[48] A. Bizzarri, "Formulation of a fault governing law at high sliding speeds: Inferences from dynamic rupture models," *Earth and Planetary Science Letters*, vol. 355356, no. 0, pp. 223–230, 11/15 2012.

[49] A. Bizzarri and S. Das, "Mechanics of 3-d shear cracks between rayleigh and shear wave rupture speeds," *Earth and Planetary Science Letters*, vol. 357358, no. 0, pp. 397–404, 12/1 2012.

[50] J. Elkhoury and L. Knopoff, "Dynamical model of faulting in two dimensions and self-healing of large fractures," *Physical review.E, Statistical, nonlinear, and soft matter physics*, vol. 86, no. 6 Pt 2, p. 066118, 2012.

[51] A. L. Goff, P. Cobelli, and G. Lagubeau, "Supershear rayleigh waves at a soft interface," *Physical Review Letters*, vol. 110, no. 23, p. 236101, 2013.

[52] K. J. Ryan and D. D. Oglesby, "Dynamically modeling fault step overs using various friction laws," *Journal of Geophysical Research: Solid Earth*, vol. 119, no. 7, pp. – 2014JB011 151, 2014.

[53] Y. Ida, "Cohesive force across the tip of a longitudinal-shear crack and griffith's specific surface energy," *Journal of Geophysical Research*, vol. 77, no. 20, pp. 3796–3805, 1972.

[54] A. C. Palmer and J. R. Rice, "The growth of slip surfaces in the progressive failure of over-consolidated clay," *Proceedings of the Royal Society of London.A.Mathematical and Physical Sciences*, vol. 332, no. 1591, pp. 527–548, April 03 1973.

[55] B. T. Aagaard, M. G. Knepley, and C. A. Williams, "A domain decomposition approach to implementing fault slip in finite-element models of quasi-static and dynamic crustal deformation," *Journal of Geophysical Research: Solid Earth*, vol. 118, no. 6, pp. 3059–3079, 2013.

[56] J. Rice and K. Uenishi, "Universal nucleation length for slip-weakening rupture instability under nonuniform fault loading," *Journal of geophysical research*, vol. 108, no. B1, 2003.

[57] T. H. Heaton, "Evidence for and implications of self-healing pulses of slip in earthquake rupture," *Physics of the Earth and Planetary Interiors*, vol. 64, no. 1, pp. 1–20, 11 1990.

[58] S. Nielsen and R. Madariaga, "On the self-healing fracture mode," *Bulletin of the Seismological Society of America*, vol. 93, no. 6, pp. 2375–2388, 2003.

[59] A. E. Elbanna, *Pulse like ruptures on strong velocity-weakening frictional interfaces : dynamics and implications. Dissertation (Ph.D.).* California Institute of Technology, Pasadena, CA, U.S., 2011.

[60] L. B. Freund, *Dynamic Fracture Mechanics.* Cambridge University Press, Cambridge, 1990.

[61] E. M. Dunham, P. Favreau, and J. M. Carlson, "A supershear transition mechanism for cracks," *Science*, vol. 299, no. 5612, pp. 1557–1559, March 07 2003.

[62] J. H. Dieterich, "Time-dependent friction in rocks," *Journal of Geophysical Research*, vol. 77, no. 20, pp. 3690–3697, 1972.

[63] A. Ruina, "Slip instability and state variable friction laws," *Journal of Geophysical Research: Solid Earth*, vol. 88, no. B12, pp. 10 359–10 370, 1983.

[64] E. Daub and J. Carlson, "Friction, fracture, and earthquakes," pp. 397–418, 2010.

[65] A. E. Elbanna and J. M. Carlson, "A two-scale model for sheared fault gouge: Competition between macroscopic disorder and local viscoplasticity," *Journal of Geophysical Research: Solid Earth*, vol. 119, no. 6, pp. 4841–4859, 2014.

[66] C. K. C. Lieou, A. Elbanna, J. Carlson, and J. M. Carlson, "Grain fragmentation in sheared granular flow: Weakening effects, energy dissipation, and strain localization," *Physical review.E, Statistical, nonlinear, and soft matter physics*, vol. 89, no. 2, 2014.

[67] C. K. C. Lieou, A. Elbanna, J. S. Langer, J. M. Carlson, and J. M. Carlson, "Shear flow of angular grains: Acoustic effects and nonmonotonic rate dependence of volume," *Physical review.E, Statistical, nonlinear, and soft matter physics*, vol. 90, no. 3, 2014.

[68] G. Zheng and J. Rice, "Conditions under which velocity-weakening friction allows a self-healing versus a cracklike mode of rupture," *Bulletin of the Seismological Society of America*, vol. 88, no. 6, pp. 1466–1483, 1998.

[69] J. P. Ampuero and Y. Ben-Zion, "Cracks, pulses and macroscopic asymmetry of dynamic rupture on a bimaterial interface with velocity-weakening friction," *Geophysical Journal International*, vol. 173, no. 2, pp. 674–692, May 01 2008.

[70] B. Allmann and P. Shearer, "Global variations of stress drop for moderate to large earthquakes," *Journal of geophysical research*, vol. 114, no. B1, 2009.

[71] R. SIBSON, "Interactions between temperature and pore-fluid pressure during earthquake faulting and a mechanism for partial or total stress relief," *Nature.physical science*, vol. 243, no. 126, pp. 66–68, 1973.

[72] A. Lachenbruch, "Frictional heating, fluid pressure, and the resistance to fault motion," *Journal of geophysical research*, vol. 85, no. NB11, pp. 6097–6112, 1980.

[73] J. Rice, "Heating and weakening of faults during earthquake slip," *Journal of geophysical research*, vol. 111, no. B5, 2006.

[74] N. M. Beeler, T. E. Tullis, and D. L. Goldsby, "Constitutive relationships and physical basis of fault strength due to flash heating," *Journal of geophysical research*, vol. 113, no. B1, 2008.

[75] H. Noda and N. Lapusta, "Three-dimensional earthquake sequence simulations with evolving temperature and pore pressure due to shear heating: Effect of heterogeneous hydraulic diffusivity," *Journal of geophysical research*, vol. 115, no. B12, 2010.

[76] R. Han, T. Hirose, T. Shimamoto, Y. Lee, and J. ichi Ando, "Granular nanoparticles lubricate faults during seismic slip," *Geology*, vol. 39, no. 6, pp. 599–602, 2011.

[77] G. D. Toro, T. Hirose, S. Nielsen, G. Pennacchioni, and T. Shimamoto, "Natural and experimental evidence of melt lubrication of faults during earthquakes," *Science*, vol. 311, no. 5761, pp. 647–649, 2006.

[78] H. Noda, K. Kanagawa, T. Hirose, and A. Inoue, "Frictional experiments of dolerite at intermediate slip rates with controlled temperature: Rate weakening or temperature weakening?" *Journal of Geophysical Research: Solid Earth*, vol. 116, no. B7, pp. – B07 306, 2011.

[79] H. Noda, E. M. Dunham, and J. R. Rice, "Earthquake ruptures with thermal weakening and the operation of major faults at low overall stress levels," *Journal of Geophysical Research: Solid Earth*, vol. 114, no. B7, pp. – B07 302, 2009.

[80] E. Brodsky, "Long-range triggered earthquakes that continue after the wave train passes," *Geophysical Research Letters*, vol. 33, no. 15, 2006.

[81] K. R. Felzer and E. E. Brodsky, "Decay of aftershock density with distance indicates triggering by dynamic stress," *Nature*, vol. 441, no. 7094, pp. 735–738, 2006.

[82] N. J. van der Elst, E. Brodsky, and E. E. Brodsky, "Connecting near-field and far-field earthquake triggering to dynamic strain," *Journal of geophysical research*, vol. 115, no. B7, 2010.

[83] D. F. C.Xu and C. J., "Identification and analysis of secondary geological hazards triggered by a magnitude 8.0 wenchuan earthquake," *JOURNAL OF REMOTE SENSING*, vol. 13, no. 4, pp. 754–762, 2009.

[84] M. Z. Hossain, C. J. Hsueh, B. Bourdin, and K. Bhattacharya, "Effective toughness of heterogeneous media," *Journal of the Mechanics and Physics of Solids*, vol. 71, no. 0, pp. 15–32, 11 2014.